On the influence of overlap topology on the tensile strength of composite bonded joints Single overlap versus overlap stacking

Kupski, J.; Teixeira de Freitas, S.; Zarouchas, D.; Benedictus, R.

DOI
10.1016/j.ijadhadh.2020.102696

Publication date
2020

Document Version
Final published version

Published in
International Journal of Adhesion and Adhesives

International Journal of Adhesion & Adhesives 103 (2020) 102696

Contents lists available at ScienceDirect

International Journal of Adhesion and Adhesives

journal homepage: http://www.elsevier.com/locate/ijadhadh

On the influence of overlap topology on the tensile strength of composite bonded joints: Single overlap versus overlap stacking

J. Kupski *, S. Teixeira de Freitas, D. Zarouchas, R. Benedictus

Structural Integrity & Composites Group, Faculty Aerospace Engineering, Delft University of Technology, Kluyverweg 1, 2629HS, NL, the Netherlands

ARTICLE INFO

Keywords:
Composite joints
Adhesive bonding
Finger joints
Joint topology
ply interleaving technique

ABSTRACT

The goal of this study is to explore new topologies for adhesively bonded composite overlap joints in order to improve their strength under tensile loading. Multiple stacked overlaps, also referred as finger joints, are compared with single overlap topologies. The quasi-static tensile behaviour of single lap joints with two overlap lengths 12.7 mm and 25.4 mm are compared to finger joints with 1 and 2 stacked overlaps through thickness with constant 12.7 mm overlap length. Two composite adherend stacking sequences are tested for each topology $[0/90]_{4s}$ and $[90/0]_{4s}$.

A non-linear FE-analysis is performed to analyse the shear and peel stresses along the adhesive bond line. A difference in peak shear and peel stress, at the tip of the bonded region could be observed: (i) for 1 finger, the peak peel stress is higher than in the single lap joint configurations because the beneficial effect of avoiding eccentricity in the finger joint is outperformed by the detrimental effect of reducing to half the adherend stiffness at the overlap; (ii) for 2 fingers, the stress field changes significantly leads to a 23% decrease in peak shear and 33% in peak peel stress, compared to the single lap joint topologies.

In addition, experimental lap shear tests are performed and monitored using acoustic emission technique, to follow the damage events. Different trends at damage initation and at maximum load are believed to result from how the damage propagates inside the joint. A topology with 2 fingers and layup $[90/0]_{4s}$, which fails entirely inside the adherend, provides the lowest peak shear and peel stress and the highest load at damage initiation. It is however outperformed in maximum load by a single lap joint topology with layup $[0/90]_{4s}$, with mostly cohesive failure. It is further found that, unlike in single overlap topologies, the most dominant stress component for damage initiation inside the finger joints is the in-plane tensile stress, at the butt joint resin pockets, rather than peel stresses at the overlap region. Lastly, if weight efficiency is the main requirement, a finger joint design can effectively replace a single overlap joint design. However, for absolute maximum joint strength, the single overlap joint is a better choice than the finger joint.

1. Introduction

Adhesive bonding is one of the most suitable joining technologies in terms of weight and mechanical performance for current CFRP aircraft fuselage structures. However, traditional joint topologies such as single overlap joints (SLJ) induce high peel stresses into the composite adherends thickness direction, resulting in sudden failure and therefore low joint strength when compared to metal adherends [1,2]. As a result, current safety-critical bonded joints are always used in combination with redundant fasteners. This practice jeopardizes the weight-efficiency of full-scale composite structures, where joints are essential.

Compared to the traditional SLJ-design, mainly chosen for its easiness of manufacturing [3], finger joints (FJ) could be a promising alternative to increase joint strength due to a more gradual load transfer to the composite adherends as they lead to lower peel stresses [1,3]. FJs, also referred as tongue-and-groove joints, are commonly used in the wood industry [4], where slots are created by profiling the bonding surface with a rotational milling tool. In Fiber Reinforced Polymers (FRP), FJs have been mostly studied for laminates with an adherend thickness above 5 mm, such as Glass Fibre Reinforced Plastic (GFRP) and sandwich structures, to connect, for example, components of wind turbine blades [5]. Sayer et al. investigated the fatigue life of secondary bonded FJ-topologies in wind turbine blades. The connection of the

* Corresponding author.
E-mail address: j.a.kupski@tudelft.nl (J. Kupski).

https://doi.org/10.1016/j.ijadhadh.2020.102696

Available online 2 August 2020

shear web to the spar caps (adherend thicknesses between 3.4 mm and 10.4 mm) of a wind turbine blade was tested experimentally and a specific FJ-topology ("Henkel UpWind Beam") was chosen to increase fatigue life over a conventional overlap joint topology [5]. Another method to create a FJ-topology is the so-called "interleaving technique" of single plies [6]. This means two adherends with overlapping fingers are laminated together, letting the plies of left and right adherend interleave each other in the joint area. This method is mainly used to join adherends with different materials, such as CFRP/GFRP or CFRP/Titanium, in one co-curing step [6].

Dvorak et al. [7] investigated secondary bonded of adhesive FJs for woven E-glass/vinyl-ester composite laminated plates to steel or other composite plates, with adherend thickness of 12.7 mm. Experimental and finite element modelling results indicated that adhesively bonded FJs between steel and composite plates, under static tensile loading condition were stronger than joints with conventional overlap topology. Matous and Dvorak focused on the stress distributions inside the FJ [8]. As in other joint configurations, they found stress concentrations at the tips of the bonded area, that depend on the local topology of the adherends. They also found a significant advantage of FJ-over conventional overlap joint topologies: Peel stresses inside the joint region remained independent from the adherend thickness. In both studies of Dvorak et al. [7,8], the FJ-topology was applied in width direction of the joint, instead of the thickness direction, as in the ply interleaving technique, with a tongue element width of 17 mm.

Canyurt et al. used genetic algorithms to improve the modelling prediction of joint strength for woven E-glass/vinyl ester laminates joined together with FJ-geometry [9]. A genetic algorithm tensile strength estimation model (GATSEM) was used to estimate the strength of secondary bonded adhesive FJs, considering overlap length (OL), bond line thickness, pre-stress near the free edges of the bond line and material type of joining parts. By optimizing the overlap length and bond line thickness, they could increase the fatigue life log(N) by factor 2.19 for CFRP/CFRP, by factor 1.82 for steel/CFRP and by factor 1.95 for aluminium/CFRP joint configurations.

Ahamed et al. developed a ply-interleaving technique for co-curing quasi-isotropic carbon/glass fibre composite materials [6]. With a quasi-isotropic stacking sequence of $[45/0/\text{-}45/90]_{2s}$ and a cured ply thickness of 0.21 mm for the CFRP and 0.26 mm for the GFRP UD-layer, the total joint thickness comprised 3.8 mm. They investigated the effect of spatial distribution of ply terminations, of longitudinal tensile modulus and of mismatching coefficients of thermal expansion for different adherends, by means of combined experimental, analytical and computational methods. The conclusion was that joint failure is caused by delamination at the location where plies terminate, as well as by transverse matrix cracking within off-axis plies.

Literature shows, that the concept of stacking overlaps through the adherend thickness is well studied as ply-interleaving technique for co-curing dissimilar materials. However, for a secondary bonding process it is so far limited to one stacking level, due to the complexity of the design. Beyond wind turbine and ship building applications with adherend thicknesses >5 mm, FJs have not been studied for secondary bonding of CFRP structures, probably because the thickness of the CFRP laminates in other applications, for example in a commercial Airbus A350-900 XWB fuselage panel, is mostly below 5 mm [10]. Furthermore, the CFRP finger slots can hardly be milled, as common milling tools still suffer enormous deterioration from processing CFRP products [11]. These manufacturing issues have so far been hindering further investigation of FJ-topologies for CFRP aircraft fuselage panels.

The aim of this study is therefore to explore the manufacturability of these type of joints in thin (<5 mm) CFRP laminates for future application in commercial aircraft structures. The study further aims to investigate whether an increase of overlap length, stacked through the thickness of the laminate, provides increase in tensile joint strength when compared to an increase of overlap length along one bond line of the SLJ-design. The ply-interleaving technique has demonstrated in previous work to increase joint strength and decrease the peak peel stress at the tips of the joint region compared to conventional overlap joints. The method is therefore chosen for this study and applied onto a secondary adhesive bonding process on monolithic CFRP adherends with aerospace-grade properties.

2. Joint design

2.1. Topology configurations

Two types of joint topologies are tested: SLJs with two overlap lengths (OL) of 12.7 mm and 25.4 mm, and FJs with one and two stacked overlaps at a constant overlap length of 12.7 mm, see Fig. 1. Specimens are built according to ASTM standard 5868–01 [12], with a constant width of 25.4 mm.

2.2. Stacking sequence

The composite adherends of these four configurations are manufactured in two cross-ply layups $[0/90]_{4s}$ and $[90/0]_{4s}$. Fig. 2 is a schematic illustration of the stacking sequence nearby the bond line region, with SLJ-topologies in Fig. 2 a) and FJ-topologies in Fig. 2 b). The variation in stacking sequence of the adherend has proven to have a significant effect on the fracture scenario of composite overlap bonded joints [13]. According to previous work from the authors, a cross-ply stacking sequence of $[90/0]_{4s}$ is expected to trigger the crack inside the composite adherends, whereas the $[0/90]_{4s}$ with 0° adjacent to the bond line is expected to limit the damage inside the adhesive [13]. The composite adherends consist of 16 UD-layers of 125 μm single ply thickness. Table 1 summarizes the total number of design configurations investigated throughout this study.

2.3. Adherend bending stiffness

The adherend bending stiffness is one of the most significant parameters that influence the peel stresses inside the adhesive bond line [13]. Therefore it is important to keep in mind that the two layup sequences $[90/0]_{4s}$ and $[0/90]_{4s}$ provide a slightly different adherend bending stiffness. Based on the classical laminate theory (CLT), the adherend longitudinal bending stiffness is determined as the flexural engineering constant of a laminate given by

$$E_x^f = \frac{12}{D_{11}^* t^3}, \tag{1}$$

for symmetric layups, with D^*_{11} being the first row/first column entry of the resulting inverse of the bending stiffness matrix, t being the overall laminate thickness and x corresponding to the direction along the joint length (longitudinal direction) [14]. Layup $[0/90]_{4s}$ has a longitudinal bending stiffness of 78.95 GPa whereas layup $[90/0]_{4s}$ has 72.70 GPa (8.6% lower).

2.4. Materials

The materials used for this study are unidirectional (UD) prepreg tapes from carbon fibres and epoxy resin for the composite adherends and an epoxy film adhesive for the bond line. The Prepreg tape is Hexply® 6376C-HTS(12K)-5-35% (Hexcel Composites in Duxford, UK), containing high tenacity Tenax®-E HTS45 standard modulus fibres (Toho Tenax Europe GmbH) and the Hexply® 6376 thermoplastic-toughened epoxy matrix system. The adhesive is Scotch-Weld™ AF 163-2K in 293 g/m^2 areal weight, including a knit supporting carrier, from 3 M Netherlands B.V. Relevant material parameters, extracted from material datasheet, as well as from previous studies with the chosen adhesive, are presented in Table 2 and Table 3. Fig. 3 shows the considered stress-strain curve for the adhesive AF163-2K taken from

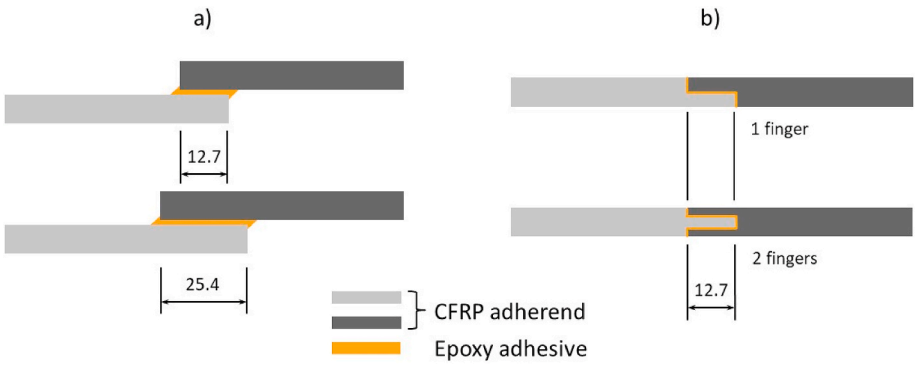

Fig. 1. SLJ-, a), and FJ-design, b), configurations, dimensions in [mm].

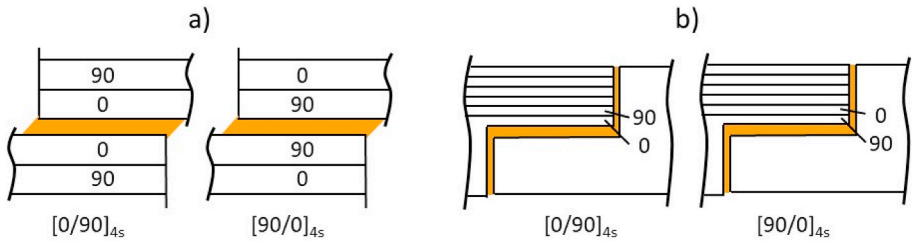

Fig. 2. Composite layup around the bond line region for the SLJ-a) and FJ-design b) configuration.

Table 1
Total number of joint configurations, with nomenclature referring to overlap topology, overlap length and layup.

Design nomenclature	Adherend's layup	overlap length [mm]
SLJ-1-90/0	$[90/0]_{4s}$	12.7
SLJ-1-0/90	$[0/90]_{4s}$	12.7
SLJ-2-90/0	$[90/0]_{4s}$	25.4
SLJ-2-0/90	$[0/90]_{4s}$	25.4
FJ-1-90/0	$[90/0]_{4s}$	12.7
FJ-1-0/90	$[0/90]_{4s}$	12.7
FJ-2-90/0	$[90/0]_{4s}$	12.7
FJ-2-0/90	$[0/90]_{4s}$	12.7

previsou studies [17]. All values are valid at room temperature (23 °C). Indices are given for different coordinate directions with "1", '2' and "3" standing for the direction along the fiber direction, transverse to the fibers and out-of-plane, respectively.

3. Stress analysis

In order to compare SLJ-to FJ-topologies in terms of stress fields surrounding the bond line, a finite element analysis (FEA) is performed with the commercial software Abaqus 2017. A comparison of the stress levels at the bond line, both in shear (τ_{xy}) and peel (σ_{yy}), gives insight on the potential of the FJ-topology, and possible limitations, in comparison with SLJ, since the peak stresses arising at the bond line tips significantly

Table 2
Material properties of Hexply® 6376C-HTS(12K)-5-35% for a UD-Prepreg layer.

Longitudinal tensile modulus	E_{11}	142000 MPa[a]
Transverse tensile modulus	$E_{22} = E_{33}$	9100 MPa[a]
In-plane shear modulus	$G_{12} = G_{13}$	5200 MPa[a]
Transverse shear modulus	$G_{23} = E_{33}/(2(1+\nu_{23}))$	3500 MPa
In-plane Poisson ratio	$\nu_{12} = \nu_{13}$	0.27[b]
Transverse Poisson ratio	ν_{23}	0.30[b]

[a] TDS of F6376 Hexcel/Airbus [15].
[b] Adapted from Hexply-8552/IM7, Camanho et al. [16].

Table 3
Material properties of Scotch-Weld™ AF 163-2K epoxy film adhesive.

Tensile modulus	E_{Adh}	2046 MPa[a]
Poisson ratio	ν_{Adh}	0.34[b]

[a] Teixeira et al. [17].
[b] TDS of Scotch-Weld™ AF 163-2K 293 g/m^2 [18].

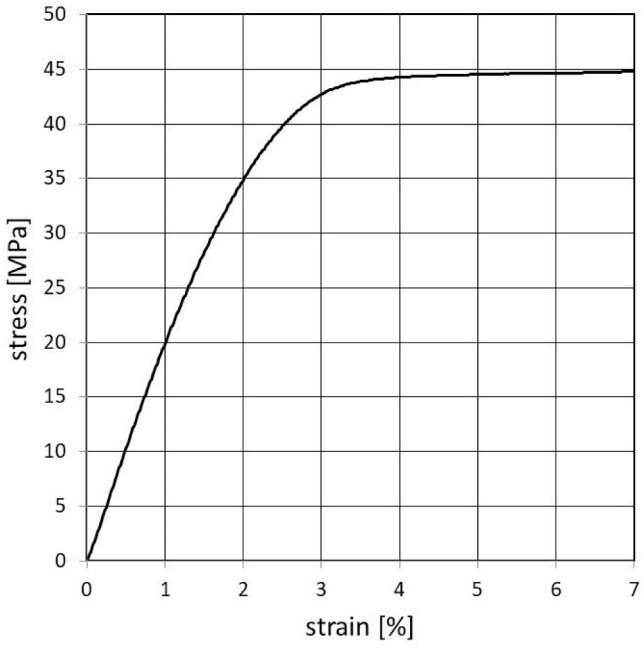

Fig. 3. Stress-strain curve of AF 163-2K 293 g/m^2 [17].

influence the overall joint strength under tensile loading [1,2].

3.1. Finite element model

Fig. 4 illustrates the model, including dimensions and boundary conditions. Each composite adherend is modelled with 16 solid elements of type C3D8 through the thickness, meaning one element per single UD-layer of 125 μm. At the right end side, the nodes are fixed in the 3 DoF (Degrees of Freedom), while on the left side, solely longitudinal displacement is allowed. Load in x-direction is applied on the left hand-side of the model. This is considered the best choice for the further comparison with the experimental results.

Fig. 5 shows the mesh at the overlap for the different topologies. Some of the assumption taken in the model, namely in terms of local topology of the bond line, are based on the visual observation of the specimens further detailed in section 4.1.2. Fig. 5a) shows the overlap area of the SLJ-1 topology with 12.7 mm overlap length (SLJ-2 topology is modelled accordingly). The spew fillet geometry is modelled as triangular fillet shape of 45° slope reaching half the adherend's height. Taking into account previous experience from the authors [13], this shape is considered to be a good approximation to represent a real spew fillet. This is further confirmed in the experimental analysis, see section 4.2. Fig. 5b) and c) show the overlap region of the FJ-topologies. Rectangular adhesive pockect at the tips of the overlap are created as an approximation of what is observed in reality, see section 4.1.2. In case of the SLJ-topologies, the bond line thickness is modelled with 150 μm thickness, whereas in case of the FJ-topologies, it is reduced to 50 μm. For the SLJ, the bond line thickness is modelled with 150 μm thickness, following results from previous work of the authors [19]. For the FJs, and equivalent adhesive thickness of 150 μm would mean that the two adjacent composite plies would either be removed or would become significantly thinner. As this is considered unrealitsic, a 50 μm bond line thickness is chosen as a good balance that does not replace a significant amount of the adjacent composite plies and would still be sufficient to guarantee adhesion between the adherends [13].

In terms of mesh size, the length and width of one element in the overlap tip region is set to 100 μm. The element width and length are progressively increased for the regions away from the overlap tip. This results in a maximum element width of 1 mm and length of 0.5 mm, at the mid-width and mid-length of the overlap, where stresses are lower. The element size towards the adherends free end is further increased for computational efficiency. In terms of thickness, in the adherend, the thickness of one element corresponds to one UD ply thickness, ie 125 μm. The adhesive layer is modelled with 2 × 75 μm through the thickness, in case of the SLJ-configurations and with 2 × 25 μm in thickness for the FJ-configurations. The mesh size of 2 element through the thickness of the adhesive is pre-determined, as it represents the smallest practical size with respect to a maximum element aspect ratio of 1:5. This results in a total mesh size of 404,352 elements for topology FJ-1, 449280 elements for FJ-2, 429,184 elements for SLJ-1 and 524,032 elements for SLJ2. A mesh convergence study is performed in order to guarantee that the results are mesh independent. For the mesh size chosen, numerical results are obtained for two types of elements C3D8 (8 nodes, linear interpolation) and C3D20 (20 nodes, quadratic interpolation). A sufficient convergence can be established with element type C3D8. The numerical results are stable (less than 5% difference) between the two mesh types. It is thereby important to note that, the convergence study holds for peel stress along the overlap length of the different configurations. In this case, stresses inside the adhesive do not reach above its yield point so that stresses tie up with the strains.

The composite is modelled as linear elastic, based on the properties listed in Table 2 [15,16], while the adhesive is modelled following the stress-strain curve obtained from tensile dog-bone tests, as shown in Fig. 3. The stress –strain curve includes both elastic and plastic behaviour of the adhesive material. The material was modelled as elastic-plastic, with 4 data points defining the stress-strain curve in the plastic regime, beginning at 25.3 MPa yield stress, and including isotropic hardening. At the pre-defined load of 1.5 kN most configurations did show no plastic strain, except for one case, FJ-1-0/90, which reached a stress peak for in-plane tensile stress above the yield point of the adhesive of 25.3 MPa. The load is applied in a single step taking into account non-linear geometry effects.

3.2. Parametric study

With the presented non-linear 3D finite element model, it is possible to explore FJ-topologies with a larger number of fingers. Fig. 6 shows the results of the parametric study of 4 topologies with increasing number of fingers: 1, 2, 3 and 7, using the layup $[0/90]_{4s}$ as an example. The particular number of fingers is a consequence of the need for a balanced layup in each finger, containing at least 4 layers of 125 μm UD-ply thickness. Fig. 6 presents the peel stress (σ_{yy}) distribution at the mid-thickness of the adhesiver along the overlap length, as this out-of-plane stress component plays the major role for damage initiation in the joint [1,2]. The plot focusses on the first 2 mm (in x-direction) from the left tip of the overlap. The FJ-1 topology has the highest peak peel stress of all configurations. With increasing number of fingers, the peak peel stress decreases, with a noticeable drop of 51%, from 7.62 MPa to 3.72 MPa between the topologies FJ-1 and FJ-2. The difference between the topologies with 2 (3.72 MPa), 3 (3.23. MPa) and 7 (2.61 MPa) overlaps is less significant with an average of 16%. The load is chosen to 1.5 kN in the parametric study.

The parametric study of Fig. 6 intends to demonstrate the potential in stress reduction for joint designs with more than 1 overlap. The peel

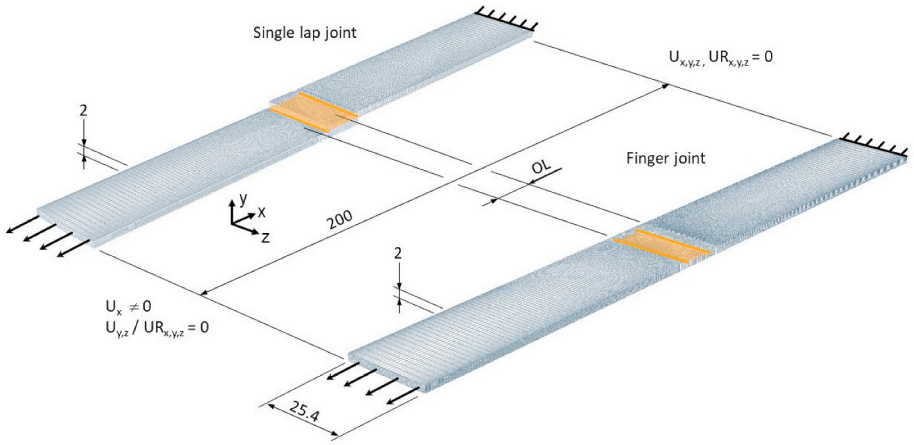

Fig. 4. 3D FE-model, SLJ design (upper left) and FJ design (lower right) with boundary conditions, dimensions in [mm].

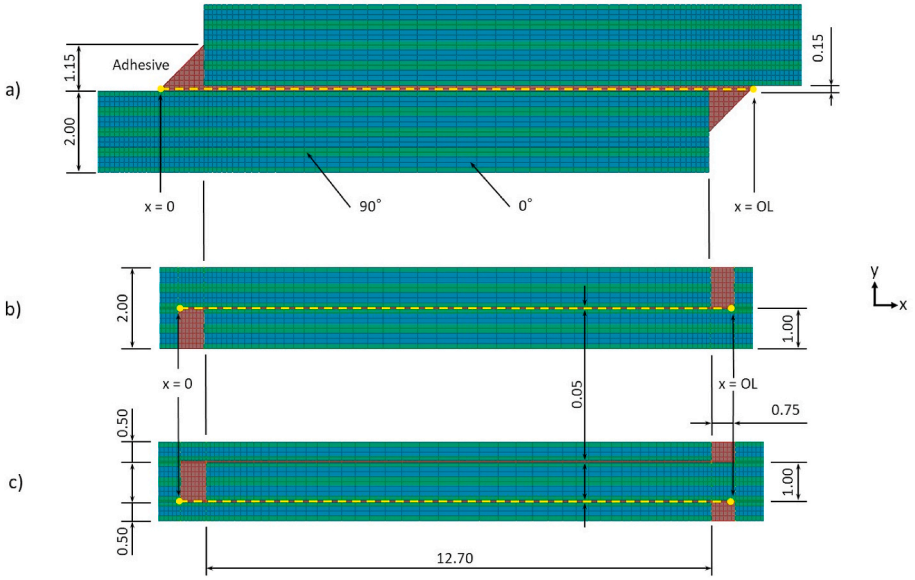

Fig. 5. 3D FE-model, central joint region, a) for SLJ design with spew fillet, b) for FJ design with 1 overlap, c) for FJ design with 2 overlaps, with layup $[90/0]_{4s}$ and dimensions in [mm].

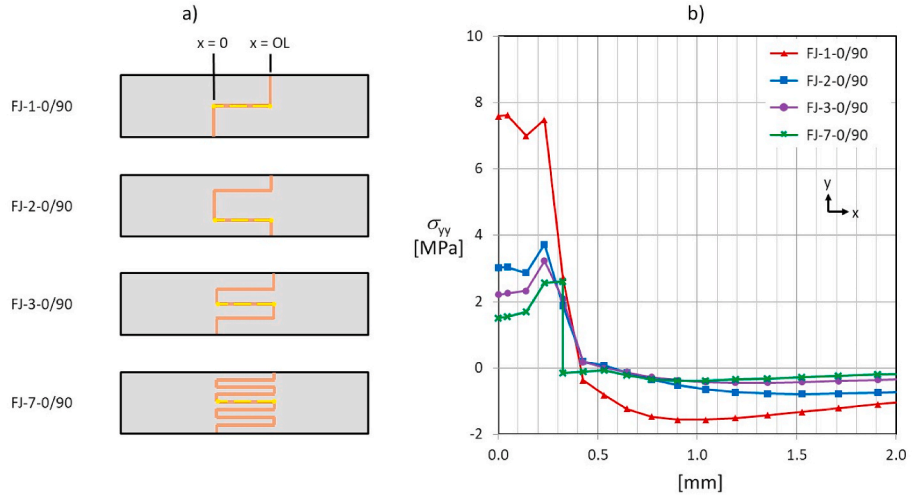

Fig. 6. Peel stress distribution along bond line length on FJ-topologies with 1, 2, 3 and 7 stacked overlaps with layup $[0/90]_{4s}$.

stress for FJ-2, FJ-3 and FJ-7 are plotted for the finger closer in terms of thickness to the location of FJ-1. However, for the remaining fingers of FJ-2, FJ-3 and FJ-7, the peak peel stress values are within the same range and all with significantly lower values than FJ-1. As a result of the parametric study it can be stated, that at least two fingers are needed to significantly decrease the peak peel stress at the bond line tip. The FJ-2-topology benefits from avoiding the eccentricity and from symmetric stress distribution, while for the FJ-1-topology the beneficial effect of avoiding eccentricity is outperformed by the detrimental effect of stiffness reduction at the overlap region. For more than 2 fingers, ie, FJ-3 and FJ-7, there is less significant stress reduction.

The general trend of all plots in Fig. 6 follows the common "bathtub curve" for SLJs, with stress peaks (in shear, peel and tensile) at the tip of the overlap region. This would explain the general plateau of the peel stress beyond x = 0.5 mm. An explanation could be, that the plateau coincides with the adhesive butt between the two composite adherends. As the stiffness is reduced in the region, the load transfer would reduce, too. However, the length of one butt is set 0.75 mm. The significant drop in peel stress in Fig. 6 is at 0.3 mm, which lies around the center of the butt, when looking in x-direction. The drop in peel stress would therefore be expected closer to one of the two interfaces in the plot path, at x = 0 mm and x = 0.75 mm.

Apparently, the total available overlap area in the FJ-2-design is sufficient to avoid large stress peaks. A load transfer over more than 2 fingers would still increase the total overlap area and therefore result in further decrease of peak peel stress, but less significantly, in context with the given joint overlap length, width and adherend thickness. A similar observation is stated in literature [1], when comparing joint strength of SLJs with increasing overlap length: At a certain threshold, the joint strength does not increase further with the increase in overlap length.

Based on these results, it is decided to focus the study on the two topologies with 1 finger and 2 fingers. Although the FJ-2-topology shows a potential for decreasing the peak peel stresses, one should also take into account the level of complexity that multiple fingers require, in terms of manufacturing and surface preparation prior to the secondary bonding process.

3.3. Stress field at the bond line region

Fig. 7 and Fig. 8 present the shear (τ_{xy}) and peel (σ_{yy}) stress

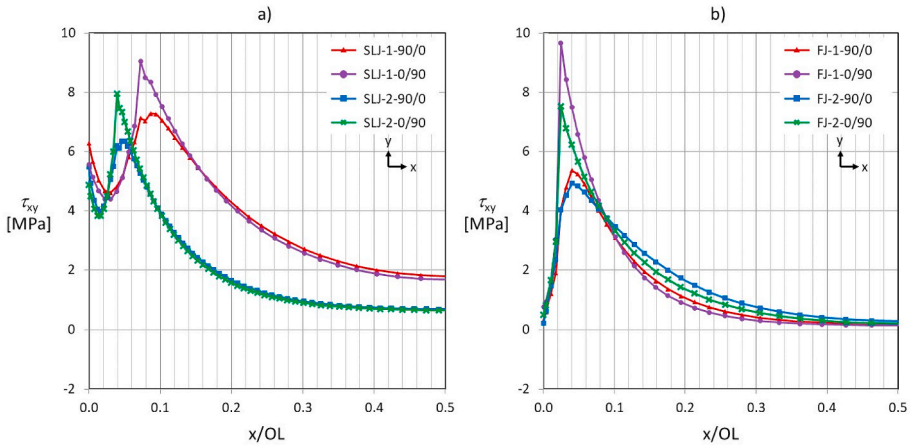

Fig. 7. Shear stress (τ_{xy}) distribution inside the adhesive along 1/2 overlap length (OL), a) for SLJ-topologies, b) for FJ-topologies.

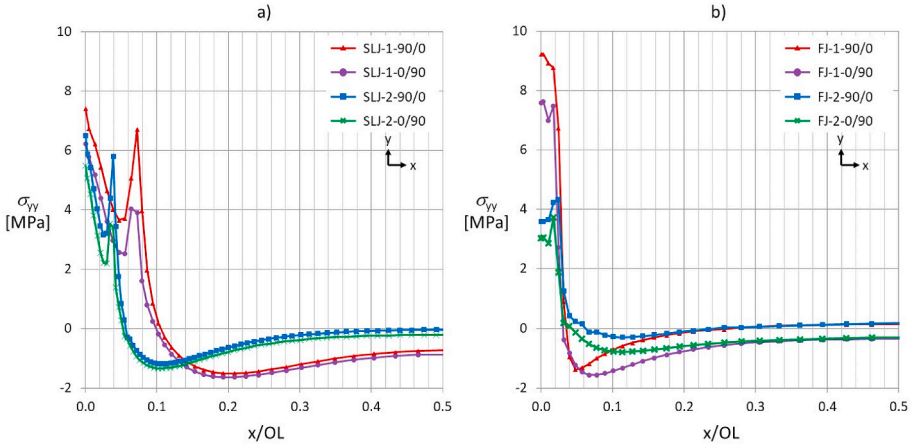

Fig. 8. Peel stress (σ_{yy}) distribution inside the adhesive along 1/2 overlap length (OL), a) for SLJ-topologies, b) for FJ-topologies.

distribution along the mid-thickness of the bond line length for both layup configurations $[0/90]_{4s}$ and $[90/0]_{4s}$ at a pre-defined load of 1.5 kN. All plots are taken at mid-width position and cover half of the bond line length. In order to compare joint topologies of different overlap lengths, the x-axis is normalized to the full overlap length (OL). The paths along which the stresses are taken, are highlighted in Fig. 5 for all topologies.

The stresses at the mid-adhesive are considered representative, as shear and peel stress do not vary significantly through the thickness of the adhesive, in comparison with the stress variation along the overlap.

The oscillatory behaviour of the shear stress in SLJs close to the bond line tips shown in Fig. 7 a) is a result of the spew fillet: The plotted stresses start just outside the actual overlap, at the end of the spew, where the lower tip of the triangle touches the lower adherend, see Fig. 5 a), x = 0. Here is the first stress peak. The second stress peak occurs when the actual overlap starts, and the upper tip of the triangle touches the upper adherend. A shift of these peaks between the different SLJs results from the different overlap lengths. So, in fact all SLJ-configurations suffer a first stress peak at the lower end of the spew fillet and a second, higher stress peak, at the upper end of the spew fillet. In case of the finger joints, the spew fillet is replaced by a shorter resin pocket, see Fig. 5b) and c). No oscillatory behaviour appears and with constant overlap length for all FJ configurations, the peaks show up at the same location along the x-axis.

The layup 0/90 always results in higher peak shear stresses in the adhesive than 90/0. This is in accordance with previous work of the authors [13], who found that an interface ply angle of 0 results in the highest shear stresses in the adhesive bond line. As the ply angle increases, the stiffness of the ply interface decreases and the shear stress inside the adhesive decreases as a consequence. From SLJ 1 to SLJ 2 and from FJ-1 to FJ-2, the peak shear stresses decrease. So, a larger overlap area decreases the peak shear stress in the adhesive in all cases.

There is no overall trend of peak shear stresses in the adhesive when comparing the two different topologies with the same layup and bonded area (plots with the same colour in a) and b)). The peak shear stress decreases by 26% from SLJ-1-90/0 (7.29 MPa) to FJ-1-90/0 (5.37 MPa), and by 23% from SLJ-2-90/0 (6.35 MPa) to FJ-2-90/0 (4.92 MPa). But the peak shear stress increases by 7% from SLJ-1-0/90 (9.06 MPa) to FJ-1-0/90 (9.67 MPa), and decreases by just 5% from SLJ-2-0/90 (7.95 MPa) to FJ-2 0/90 (7.54 MPa).

FJ-1 results in the highest peak peel stresses at the bond line tips. It is therefore the topology that will most likely promote early delamination in the composite adherends. FJ-2 results in the lowest peak peel stress at the bond line tips. It is consequently expected to be a promising topology to delay delamination in the composite adherend and increase the strength of the bonded joint. SLJ-1 and SL-2 result in similar peak peel stress at the bond line tips. These values lie between the FJ-1 and FJ-2. In case of the FJ-2 configurations, the peel and shear stress distribution in both overlaps are very similar.

The change from FJ to SLJ has two conflicting effects on the stress field at the overlap. On one hand, by elimating the eccentricity between the adherends from SLJ to FJ, the detrimental secondary bending moment at the overlap is eliminated. This leads to a smaller rotation of the joint and a decrease in peel stresses, at the bond line tip. On the other

hand, the stiffness of the adherend at the overlap region is reduced from full adherend thickness in the SLJ-to half adherend thickness in the FJ-topology. This reduction in tensile and bending stiffness at the overlap area leads to higher local deformation causing an increase in peel stresses.

Therefore, for the FJ-1-topology the beneficial effect of avoiding eccentricity is outperformed by the detrimental effect of stiffness reduction, so that the peak peel stress is higher in this topology than in the SLJ-configurations. For the FJ-2-topology, the scenario changes significantly. In this case the FJ-2-topology outreaches the SLJ-topologies. The peak shear stress decreases by 23%, from SLJ-2-90/0 (6.35 MPa) to FJ-2-90/0 (4.92 MPa) and the peak peel stress by 33% from SLJ-2-90/0 (6.51 MPa) to FJ-2-90/0 (4.34 MPa). Furthermore, it is interesting to note that in terms of layup, $[0/90]_{4s}$ results in higher peak shear stress but lower peak peel stress when compared to $[90/0]_{4s}$. This is in accordance with previous studies of the authors [13], which found that an interface ply of 0° in contact with the adhesive results in high shear but low peel stress inside the bond line, causing the joint to fail cohesively.

To summarize, Table 4 presents peak shear ($\tau_{xy,max}$) and peel ($\sigma_{yy,max}$) stress inside the adhesive, that are derived from the numerical 3D-FE model along the bond line length, as well as the peel-to-shear ratio of those. The peel stress, as an out-of-plane stress, causes a mode-I crack opening mode, which requires the lowest amount of energy for a crack to propagate [2]. Therefore it is of great interest to achieve a low peel-to-shear ratio.

In the FJ-configurations, the vertical butt joints are modelled with the same isotropic adhesive material properties as the flat overlaps, see Fig. 5b) and c). So, they represent a very ductile gap-filler, which is perfectly connected to the adjacent CFRP layers. However, at this location the adhesive suffers from in-plane tensile stresses, as in a butt joint, which could be critical for the failure initiation of the FJ-configurations. It is therefore important to have a closer look onto these in-plane tensile stresses at the butt joints. Fig. 9 shows the in-plane tensile stress at the butt joints for the FJ-topologies. The stresses are plotted at the interface between adhesive and adherend (in x-direction) where stresses are found to be highest, from bottom of the adherend till the center (in y-direction) and at mid-width (in z-direction). When comparing the values for τ_{xy} and σ_{yy} in Fig. 7 b) and Fig. 8 b) with σ_{xx} in Fig. 9 b), it is observed that for FJs the in-plane tensile stresses at the butt joints are the most critical rather than the peel stresses in the overlaps. For the FJ-1-configurations, FJ-1-90/0 has 24.3 MPa in σ_{xx}, compared to 5.37 MPa in τ_{xy} and 9.45 MPa in σ_{yy} and FJ-1-0/90 has 28.1 MPa in σ_{xx}, compared to 9.67 MPa in τ_{xy} and 7.77 MPa in σ_{yy}. For the FJ-2-configurations, FJ-2-90/0 has 10.0 MPa in σ_{xx}, compared to 4.92 MPa in τ_{xy} and 4.34 MPa in σ_{yy} and FJ-2-0/90 has 10.4 MPa in σ_{xx}, compared to 7.54 MPa in τ_{xy} and 3.72 MPa in σ_{yy}. All numbers are summarized in Table 4.

Table 4
Peak shear ($\tau_{xy,max}$), peel ($\sigma_{yy,max}$), peel-to-shear ratio ($\sigma_{yy,max}/\tau_{xy,max}$) for all configurations and peak tensile ($\sigma_{xx,max}$) stresses in the butt region for FJ-configurations.

	Peak shear stress	Peak peel stress	Peel-to-shear ratio	Peak tensile stress in butt region
	$\tau_{xy,max}$ [MPa]	$\sigma_{yy,max}$ [MPa]	$\sigma_{yy,max}/\tau_{xy,max}$ [−]	$\sigma_{xx,max}$ [MPa]
SLJ-1-90/0	7.29	7.42	1.02	
SLJ-1-0/90	9.06	6.23	0.69	
SLJ-2-90/0	6.35	6.51	1.03	
SLJ-2-0/90	7.95	5.50	0.69	
FJ-1-90/0	5.37	9.45	1.76	24.3
FJ-1-0/90	9.67	7.77	0.80	28.1
FJ-2-90/0	4.92	4.34	0.88	10.0
FJ-2-0/90	7.54	3.72	0.49	10.4

Two more observations can be made from Fig. 9: 1) The in-plane tensile stresses at the butt joints in FJ-1 configurations show an oscillatory behavior, which results from layup orientation: Higher tensile stresses inside the adhesive at the adhesive-adherend interface are aligned with the fiber-dominated stiffness of a 0 °-ply and lower tensile stresses are aligned with the matrix-driven stiffness of a 90 °-ply. This is a complementary finding to previous conclusions from the authors, stating that 0° as an interface ply in a SLJ-configuration results in the highest shear stresses inside the adhesive [13]. 2) It is interesting to note that the tensile stresses σ_{xx} at the mid adherend thickness converge to the same value for both configuration FJ-1 and FJ-2, around 10 MPa. This could be relate to what was found in the parametric study presented in Fig. 6 of previous subsection 3.2. At the mid adherend thickness, the tensile stress level inside the FJ-topologies may reach a plateau, independent from layup and number of overlaps.

It is well known [1] that an increase of overlap length in a SLJ does not decrease peak stresses in peel and shear by the same amount, which is in agreement with the observations in Fig. 7 a) and Fig. 8 a) on the SLJ-configurations. This law of diminishing returns has to do with the load transfer in a SLJ and relates to the length of the overlap, but not the overlap area. So, with 2 bond lines in FJ-2, which is the same bond line length as in FJ-1, the shear stress is expected to cut in half. However, by looking at Fig. 9, this is not the case. Assuming that any load transmitted across the butts is removed from the overlap region, the load in the FJ-1 transmitted by the butts is higher than in the FJ-2 configuration. Consequently, the overlap in the FJ-1 has to carry less remaining load than in the FJ-2.

It can be stated that in practice the butts will fail first, as the in-plane tensile stresses, seen in Fig. 9, are higher than the peel and shear stresses. Therefore, the joint performance should be linked to the butt stresses instead of the overlap stresses.

Taking into account this stress analysis, it is expected that the difference in lap shear strength follows the trend that is observed in the stress analysis, meaning that FJ-2 would outperform the SLJs in maximum load, while the topology with 1 finger (FJ-1) would reach lower maximum load than the SLJs. Those joint topologies with layup $[0/90]_{4s}$ are expected to fail cohesively inside the adhesive, when compared to layup $[90/0]_{4s}$, as the higher stiffness of the adjacent layer would trigger a crack to propagate inside the adhesive [13].

4. Experimental analysis

In the previous section, the stress analysis has shown a potential for finger joint topologies, from 2 fingers onwards, to decrease peel stress at the tip of the bond line. Consequently, the question could be raised, if this observation is only valid for the linear-elastic region below the load where the damage initiates. How will the topology and the layup affect the damage resistance of the joint and the joint strength till final failure? An experimental campaign can help validate the linear-elastic model and can give more insights into the damage evolution inside the joint beyond damage initiation. Furthermore, since the finger joint topology is known to be fairly complex in terms of manufacturing, an experimental campaign can also prove or disprove its feasibility.

4.1. Specimen manufacturing

In order to create lap shear specimens according to ASTM standard 5868–01, adherends are laminated in a Prepreg hand layup process, with 15 min of de-bulking at an under pressure lower than 100 mbar. As recommended by the manufacturer of the chosen Prepreg system Hexply® 6376C-HTS(12K)-5-35%, intermediate debulking sessions are

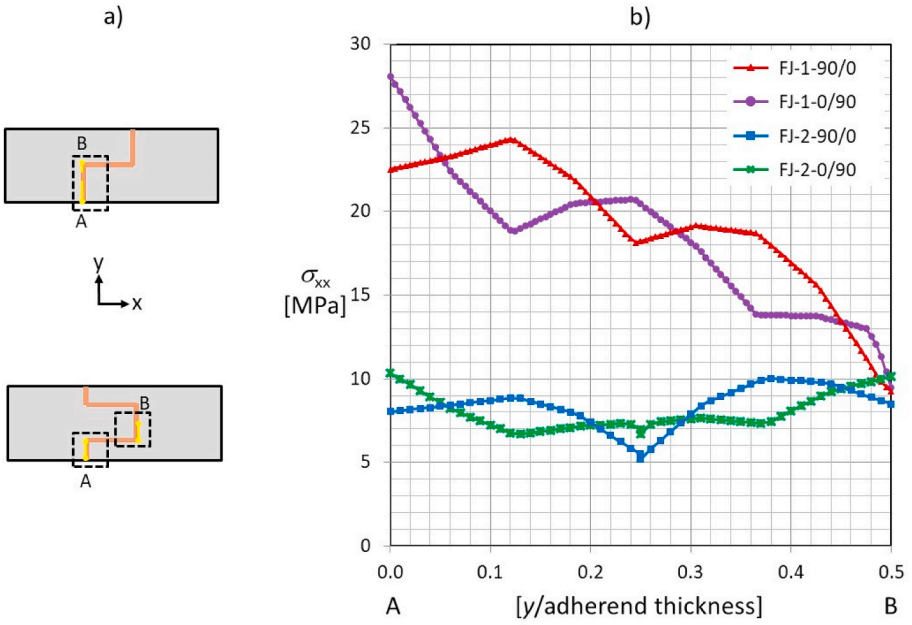

Fig. 9. Longitudinal tensile stress distribution, plotted at the outside interface between adhesive butt joint and adherend, from bottom till center of the adherend.

performed after every 4th layer, before curing inside the autoclave [15]. The laminates are placed between a base plate of 12 mm thickness and a caul plate of 2 mm thickness from aluminium. Fig. 10 illustrates the sequence for manufacturing the specimen. In order to minimize resin flow-out along the edges of the laminate, an aluminium barrier is added during the autoclave curing cycle.

Fig. 11, below, shows a close-up of the aluminium liner, which is placed at the edge of the laminate during the layup process. The sheet mimics the thickness of 4 cured layers (4 × 125 µm = 500 µm) and both its upper and lower side are carefully grinded to reach a repeatable surface roughness of 10 µm (hand-held rotational grinding machine with grain size 80/180/240, 2 min each with constant movement in 0/90 °-direction). In addition to the liner, a Teflon coated release foil is added to the layup, in order to improve release ability. The release foil's thickness of 50 µm is taken into account for the creation of fingers. The autoclave curing process comprises a single dwell step at 177 °C and 7 bar gauge pressure, with 800 mbar underpressure inside the vacuum bag for 120 min time.

Thereafter, a secondary adhesive bonding process is performed by laying the uncured film adhesive onto the cured adherends and arranging a vacuum setup around them. Prior to bonding, a surface treatment is applied to the CFRP surface which consists of the following procedure: (1) degreasing the surface with Acetone, (2) manual grinding with 3 M's Scotch Bride™, (3) cleaning with Acetone, and (4) 7 min UV/ozone treatment [20,21]. Previous studies have shown that this surface treatment results in good wettability of the CFRP surfaces [22]. The bonding curing process is performed in the autoclave at 2 bar gauge pressure and 120 °C curing temperature for 90 min dwell time, while venting the vacuum bag to full atmosphere.

The assembly of the FJ-2 topologies needs special care, in order to avoid any disruption of the film adhesive. Spreading clamps are used to open the embracing adherend side lightly (right adherend in Fig. 1 b) at FJ-2). This is done with care, to prevent accidental crack initiation inside the joint by excessive spreading.

4.1.1. Process tolerances

After curing, adherends of the SLJ-designs have a consistent thickness of 2.0 mm (±0.1 mm) of the CFRP laminate and 0.15 mm (±0.10

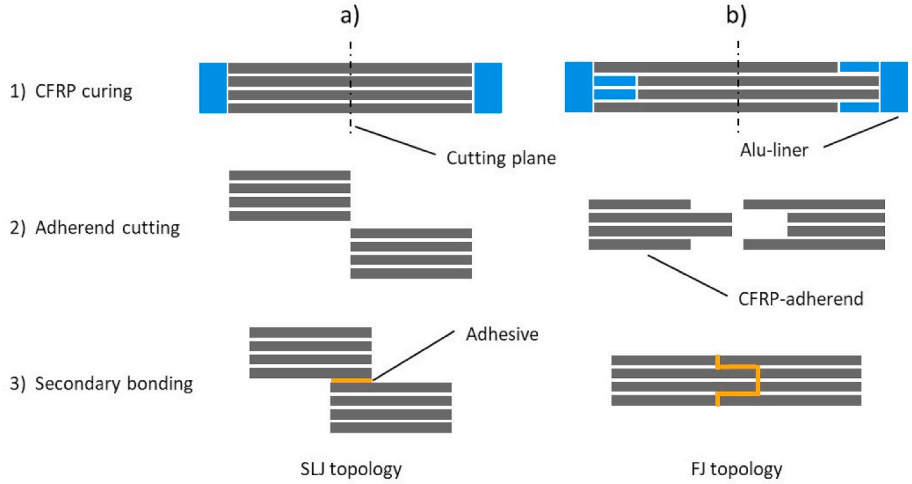

Fig. 10. Manufacturing sequence for a SLJ-, a), and a FJ-topology with 2 fingers, b), with integrated aluminium liners (in blue). (For interpretation of the references to colour in this figure legend, the reader is referred to the Web version of this article.)

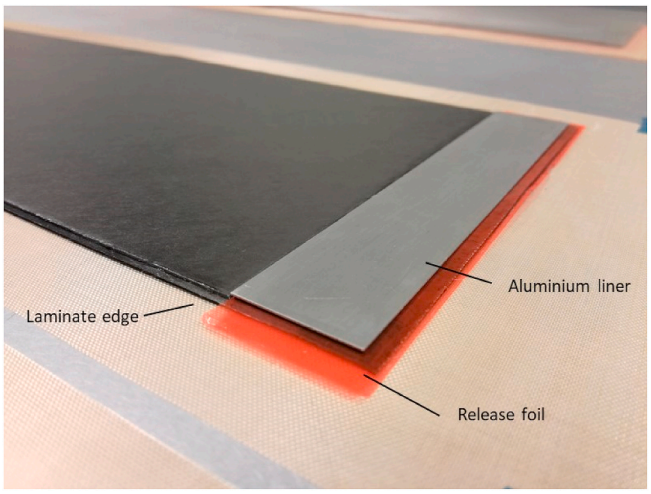

Fig. 11. Laminating CFRP plate for FJ-2-90/0 (2 fingers with layup $[90/0]_{4s}$) with integrated aluminium liners and release foil.

mm) of the bond line. In case of the FJ-specimens, the average thickness of the laminate at the overlap region decreases at the joint region by 23% (from 2.15 mm mm to 1.65 mm) in the $[90/0]_{4s}$ layup and by 15% (from 2.07 mm to 1.75 mm) in the $[0/90]_{4s}$ layup.

Fig. 12 illustrates the overlap region of the CFRP adherend of a FJ-2-90/0 design prior to bonding. There is a noticeable decrease in cured laminate thickness from the center of the adherend (right side) towards the interleaving fingers (left side). The laminate thickness of the finger with layup $[90/0]_{4s}$ decreases to 0.8 mm, instead of the expected nominal value of 1.0 mm. This effect is caused by a significant amount of resin flow-out during the fabrication of the adherends. A zone of decreased laminate thickness is visible along all surrounding edges of the CFRP-plates. This flow-out zone has a width of 40 mm, measured from the plate edge towards the center of the plate. Resin flow barriers are used to contain all resin at the edges. However, a decrease in total adhered thickness of 8%, from 1.94 mm to 1.79 mm, is observed, as shown in Fig. 12. This resin flow-out would promote higher fiber volume content at the edge of the specimen, which consequently results in a change in material properties. Fig. 13 shows the same FJ-2-0/90-configuration as in the previous Fig. 12, after the secondary bonding process. Fiber undulations develope in the vincinity of the finger dent. Steps between different plies are visible near the bond line region, giving shape to the right side of the adhesive pocket in Fig. 13 b). All thickness values are measured with a digital micrometer with an accuracy of 1 µm, while the overlap length was measured with a digital caliper of accuracy 10 µm.

Fig. 14 shows typical examples of specimens of the other topologies studied, the SLJ-1 in Fig. 14 a) and the FJ-1 in Fig. 14 b). Compared to the FJ-2-topologies presented above, the FJ-1 topologies exhibit less of the observed manufacturing flaws due to the lower complexity of the joint topology and the SLJ-topologies show no noticeable manufacturing flaws at all.

4.1.2. Surface analysis

A surface analysis using contact angle measurements is performed to the pre-treated CFRP surfaces to assess their wettability. The contact angle of a 4 µl distilled water drop is measured, having a topology imprint from the aluminium base and caul plate with 10 µm surface roughness, using the Technex Cam200/Attension Theta V4.1.9.8 system. The combined surface treatment of Acetone degreasing and exposure to UV-light in an ozone-containing atmosphere reduces the value of the contact angle by 78%, from 91° (±3°), before treatment to 20° (±1°), after treatment, for the SLJ design configuration. Due to poor surface accessability in case of the FJ design configurations, the value of the contact angle reduces only 54%, from 76° (±4°), before treatment to 35° (±5°), after treatment. Nevertheless, the contact angle values after pre-treatment are in accordance with literature and correspond to a sufficient wettability of the surface [22].

4.2. Experimental setup

Five specimens per design configuration are subjected to quasi-static tensile loading. The tests are performed under displacement control with a constant displacement rate of 1.3 mm/min, according to the given ASTM test procedure [12]. The tests are performed on a Zwick-Roell AllroundLine Z250 SW testing machine with a load cell of 250 kN.

Fig. 15 shows a schematic illustration of the test set up. Specimens are clamped at the ends by two clamps at 250 bar hydraulic pressure. The initial distance of the clamps is set to 200 mm. For the SLJ-configurations, the clamps are set to a misalignment of 2 mm to counterbalance the overlap offset. For the FJ-configurations no offset is needed. Beyond recording the load and displacement from the testing machine, an Acoustic Emission (AE) system by Vallen Systeme GmbH is employed, consisting of two VS900-M sensors, to monitor the acoustic emission activity during the tests. The AE system is connected to the load cell of the test frame in order to synchronize the AE activity with the load measurements. The AE-sensors are attached onto the same side of the specimen at ± 30 mm from the overlap centre and connected to an AEP4H 34 dB amplifier.

4.3. Load - displacement curves

Fig. 16 shows the representative load-displacement curves for each topology configuration. Fig. 16 a) shows the four configurations with SLJ-topologies, while Fig. 16 b) presents for the configurations with the FJ-topologies. In Fig. 16 a), the SLJ2-0/90 reaches significantly higher ultimate load than the other three topologies. In Fig. 16 b) The FJ-2-90/0, unlike any other configuration, is able to carry load after the first load drop at 1.5 mm displacement and reaches its ultimate load of 16.5 kN at a displacement of 2.5 mm. All plots in Fig. 16 show a similar initial slope and, except for the FJ-2-90/0 in Fig. 16 b), a sudden final failure. The FJ-2-90/0 presents a load drop and subsequent increase on the load-displacement response. This is representative of all 5 specimens tested of this configuration.

Table 5 presents the average maximum load and correspondent displacement for each configuration. In average, the maximum load ranges from 7.10 kN for the SLJ-1 $[90/0]_{4s}$ to 20.03 kN for the SLJ-2 configuration with $[0/90]_{4s}$ layup. The work in the load-displacement curves allows a comparison of average energy until failure for the

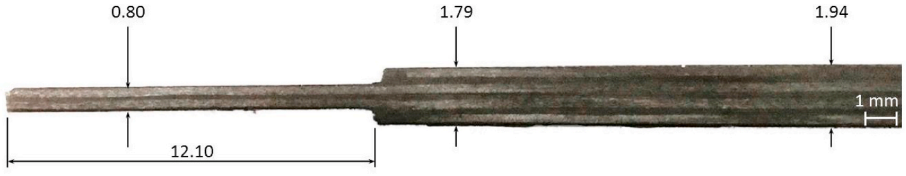

Fig. 12. Variation in layup thickness at the overlap region of finger joint with 2 fingers (FJ-2-) and layup $[90/0]_{4s}$ prior to bonding, under optical microscope with 1× magnification, dimensions in [mm].

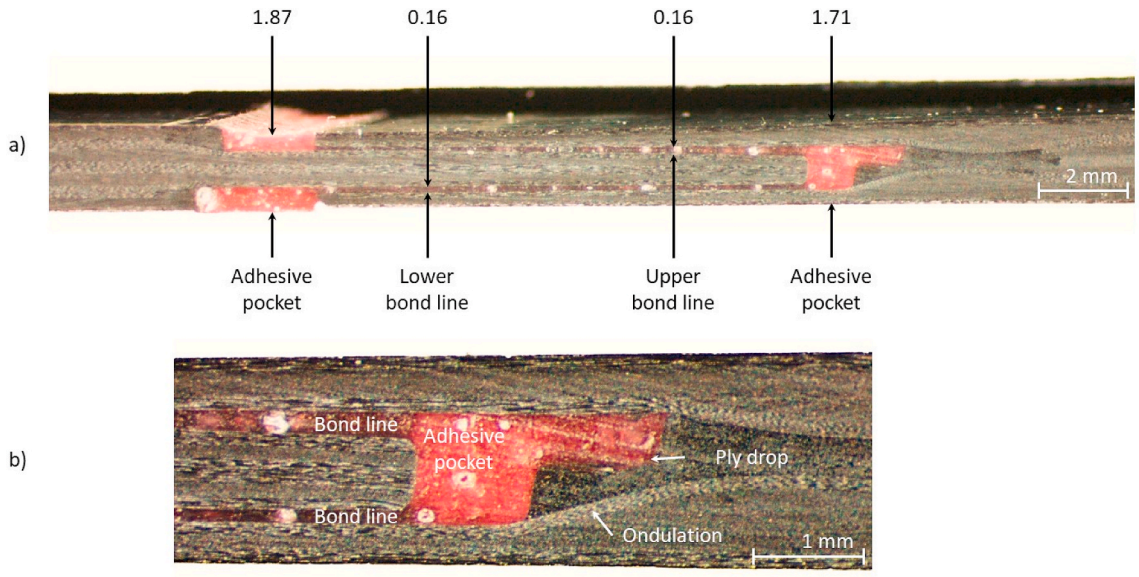

Fig. 13. a) Overlap region of FJ-2-0/90 after bonding, dimensions in [mm]
b) Zoom in of the righthand side adhesive pocket.

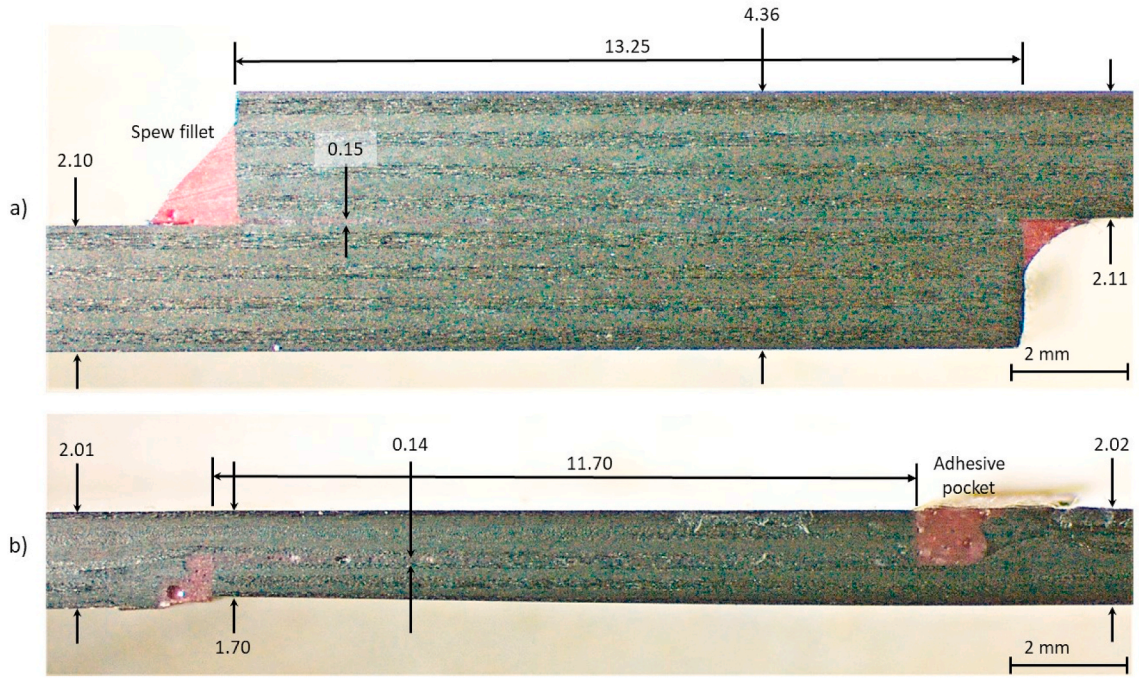

Fig. 14. Overlap region of a) SLJ-1-90/0, and b) FJ-1-0/90, after bonding, dimensions in [mm].

different configurations, by determining the area under the load-displacement. The results are presented in Table 5, ranging from minimum 2.88 (±0.86) x 10^6 J for the SLJ-1-90/0 to maximum 17.98 (±1.66) x 10^6 J for the SLJ-2-0/90 type.

It can be seen from the load-displacement curves of Fig. 16, that the joint stiffness of different configurations is in close range. The SLJs in Fig. 16 a) show a 6% higher average joint stiffness of 10.7 kN/mm compared to the FJs with 10.1 kN/mm average joint stiffness in Fig. 16 b).

The last column in Table 5 presents the average load at damage initiation for each joint configuration. Acoustic Emission (AE) technique is used to monitor the damage events during the experimental campaign. A sudden increase of AE-energy is chosen as indicator for damage initiation, as follows:

$$E^{AE}{}_i > 10^{-13}\ \text{J AND } E^{AE}{}_{i+1} \leq 10^{-8}\ \text{J}, \quad (2)$$

With E^{AE} being the acoustic energy per hit (i). Damage initiation is believed to cause a significant increase in AE-energy. But it is not clear a-priori, what would be the threshold in absolute numbers, as for each test-campaign the AE-signal depends from the Young's Modulus and density of the chosen materials in the specimen. Therefore, AE-data are evaluated in 3 steps:

1) Exclude any AE-activity in the first 10% of maximum load, due to clamping, specimen rectification or other machine setup noise at the beginning of the test.

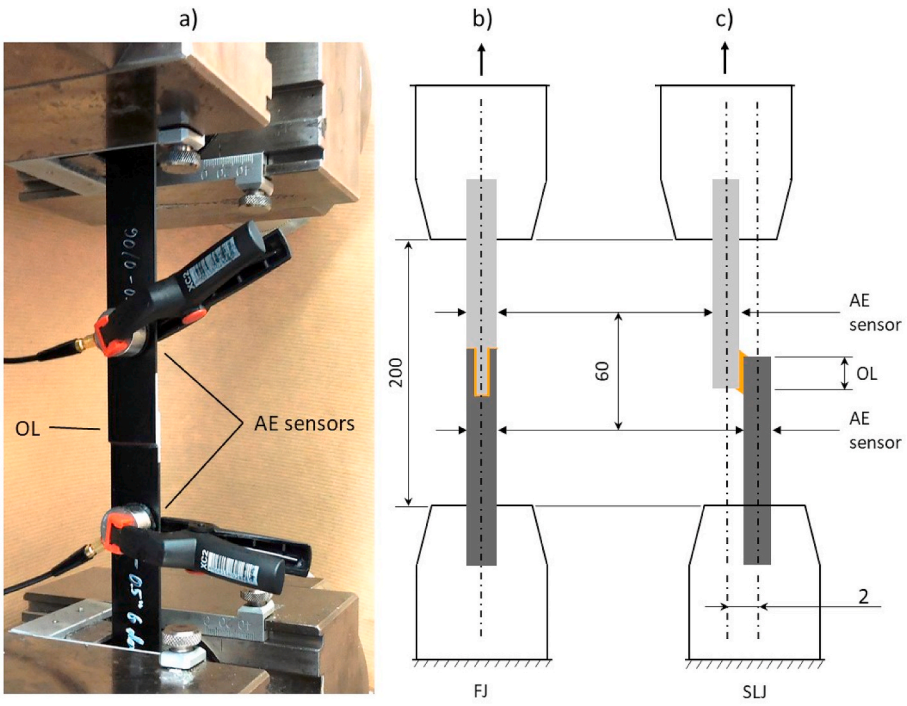

Fig. 15. Experimental test setup (a), and schematic illustration for FJ-, b), and SLJ-joint topology with clamping offset, c), dimensions in [mm].

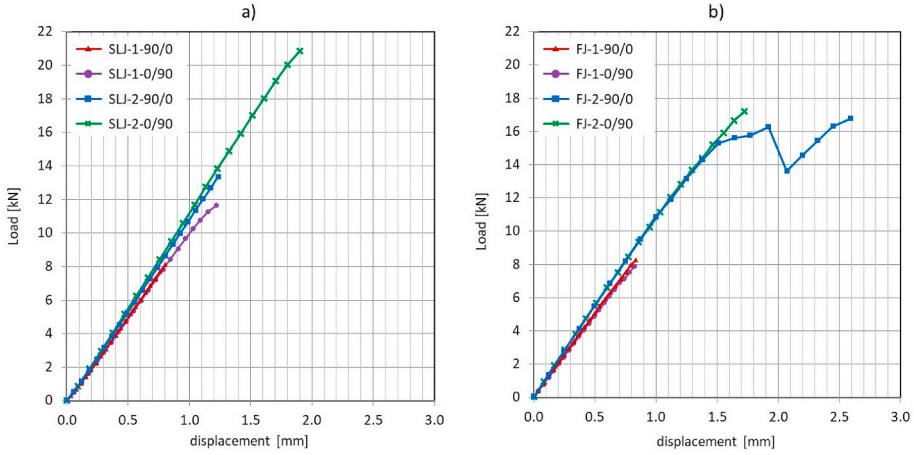

Fig. 16. Load-displacement curves, a) with SLJ-topologies, b) with FJ-topologies.

2) Neglect AE-activity at the very end of the load displacement curves. Based on previous work, it is assumed, that damage initiation for this specific set of adherend/adhesive SLJ, is expected to happen below 90% of maximum load [13.]
3) For the remaining data, find the largest increase in AE-energy, for both sensors. Comparing this largest increase factor in all specimens, find a common multiple over all cases.

For the parametric study, the mesh convergence and the stress analysis, a consistent design load of 1.524 kN (30 N/mm2 surface traction x 2 mm specimen height x 25.4 mm specimen width) was chosen. On the crosshead of the tensile machine, the maximum load was measured 7.099 kN mean value over 5 specimens for the weakest configuration, SLJ-90/0 with 12.7 mm overlap length. Comparing these two, the numerical design load can then be described as 1.524/7.099 = 21.47% of average maximum load of the weakest configuration. The load of damage initiation, indicated by Acoustic Emission technique in Table 5, is in all cases well below final failure, at most 30% in case of FJ-2-90/0, minimum at 10% in case of the SLJ-2-0/90 and in average at 21% of the maximum load. The numerical design load lies below the experimental damage initiation load in most configurations, except for one case, FJ-1-0/90, which was indicated with a very low damage initiation load at 1.2 kN average. With design load of 1.5 kN in the models, most configurations did not show any plastic strain, except for one case, FJ-1-0/90, which reached an in-plane tensile stress of 28.1 MPa, which lies above the yield point of the adhesive of 25.3 MPa, see Fig. 9.

4.4. Fracture surfaces

Fig. 17 shows the typical fracture surfaces for the four SLJ-topology configurations. The SLJ topologies SLJ-1-90/0 and SLJ-2-90/0 in Fig. 17 a) and c), show interlaminar failure inside the composite, between 1st (90°) and 2nd layer (0°) and no trace of cracks propagating throught the adhesive bond line. In the case of SLJ-2-90/0, the crack splits up at ca. 40% of overlap length and jumps perpendicular to the bond line

Table 5
Load at damage initiation [kN], maximum load [kN], displacement at maximum load [mm] and work [10^6 J].

	Maximum load	Displacement at maximum load	Work	Load at damage initiation
	F_{max} [kN]	d [mm]	W [10^6 J]	F_{init} [kN]
SLJ-1-90/0	7.10 (±0.73)	0.71 (±0.08)	2.88 (±0.86)	1.95 (±0.54)
SLJ-1-0/90	11.17 (±0.41)	1.18 (±0.08)	6.55 (±0.55)	2.25 (±0.12)
SLJ-2-90/0	12.57 (±0.62)	1.17 (±0.05)	7.50 (±0.67)	3.03 (±0.60)
SLJ-2-0/90	20.03 (±0.84)	1.79 (±0.11)	17.98 (±1.66)	2.08 (±0.41)
FJ-1-90/0	7.99 (±0.35)	0.82 (±0.02)	3.20 (±0.14)	1.20 (±0.07)
FJ-1-0/90	8.45 (±0.75)	0.89 (±0.11)	3.68 (±0.73)	1.56 (±0.36)
FJ-2-90/0	15.88 (±1.29)	2.48 (±0.39)	14.13 (±3.27)	4.78 (±0.41)
FJ-2-0/90	15.24 (±2.28)	1.49 (±0.25)	11.23 (±3.06)	2.82 (±0.83)

thickness until reaching between 1st (90°) and 2nd (0°) layer of the opposite adherend again. The SLJ-1-0/90 configuration in Fig. 17 b) results in a mixed fracture surface with a crack partly propagating through the adhesive and partly along the 1st layer (0°) (intraply failure) adjacent to the bond line. For the SLJ-2-0/90 in Fig. 17 d) cohesive failure inside the adhesive is mostly observed.

Fig. 18 shows the typical fracture surfaces for the FJ-topology. The first three configurations in Fig. 18a)–c) show a failure pattern with interlaminar failure inside the composite. The crack is believed to initiate at the interface between 1st (90°) and 2nd layer (0°) away from the bond line. In Fig. 18 d), crack pathes are observed on both embracing fingers as a mix of interlaminar failure between 1st (0°) and the 2nd (90°) outside layer and intralaminar failure inside the most outside (0°) layer.

The failure pattern in Fig. 18 would be in good agreement with observations of Ahamed et al. [6], who investigated the ply-interleaving technique for joining dissimilar composite materials, using combined experimental, analytical and numerical methods. They stated that joint failure is caused by delamination at the location where plies terminate, as well as by transverse matrix cracking within off-axis plies. Overall, all configurations with layup $[90/0]_{4s}$, exhibit final fracture surface inside the composite. FJ-topologies with layup $[0/90]_{4s}$ fail inside the composite, while SLJ-designs of the same layup fail inside the adhesive.

Post-mortem fracture surface analysis is performed using the Keyence VR5000 Wide-area 3D profiling system. This surface analysis indicates in which ply the failure inside the composite adherend occurs and, as a consequence, if it is intra- or interply failure. This information enables to draw the crack profiles, presented in Figs. 17 and 18. Fig. 19 shows as an example the top adherend side of a typical SLJ-1 configuration in layup $[0/90]_{4s}$. The final fracture surface is presented as a 3D profile. A cross section profile along the length of the overlap is also shown below the 3D profile. Two height profiles throughout the overlap region give an idea where the crack has travelled through the laminate. In the same way, Fig. 20 shows as an example the top adherend side of a typical FJ-1 configuration in layup $[90/0]_{4s}$.

In Fig. 18, the FJ-2-90/0 configuration presents a clean interply failure, together with a lower damage resistance, compared to the FJ-2-0/90, with a more complex crack path between first and second layer. At this point, there is not enough evidence to show whether the crack in the FJ-2-0/90 developed from the inside, branching into several paths and thereby providing higher damage tolerance. It is therefore important to note that, the stress analysis of Figs. 7–9, in subsection 3.3 can only link with damage initiation, not with final failure and subsequently final fracture surfaces.

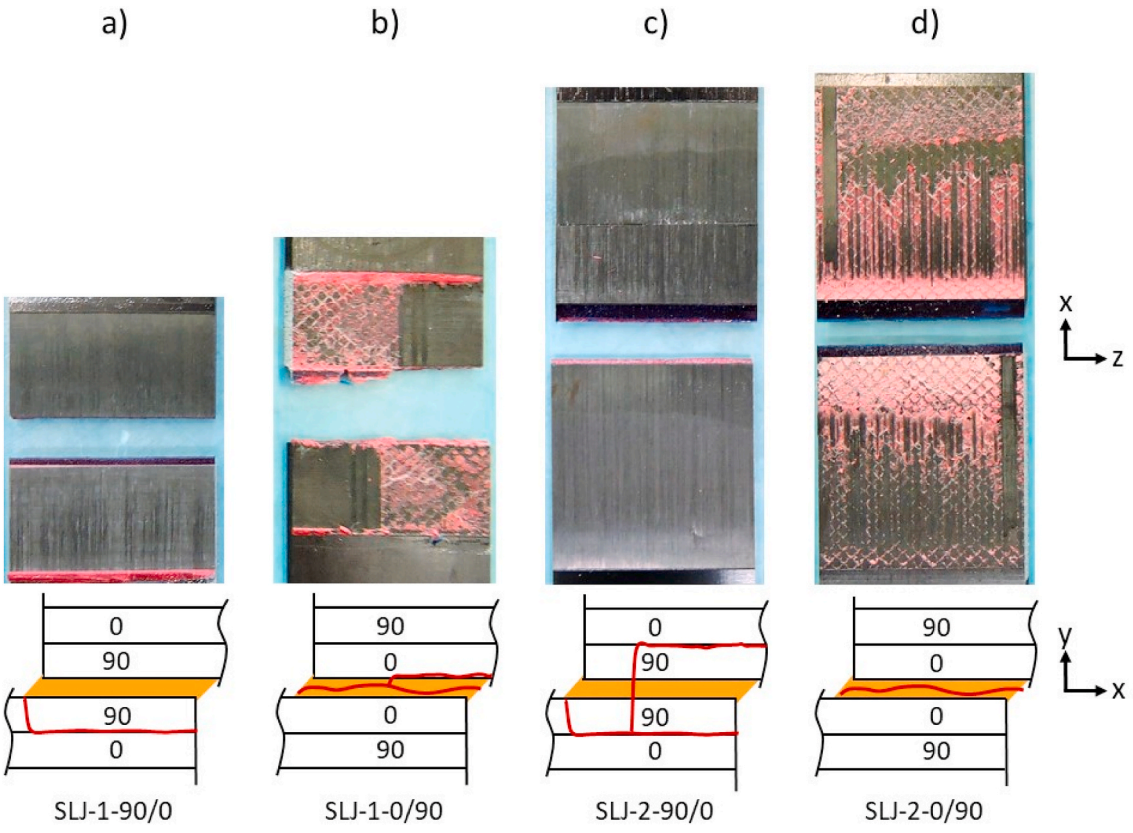

Fig. 17. Final fracture surfaces of SLJ-topologies with layup $[90/0]_{4s}$ (a–b) and layup $[0/90]_{4s}$ (c–d).

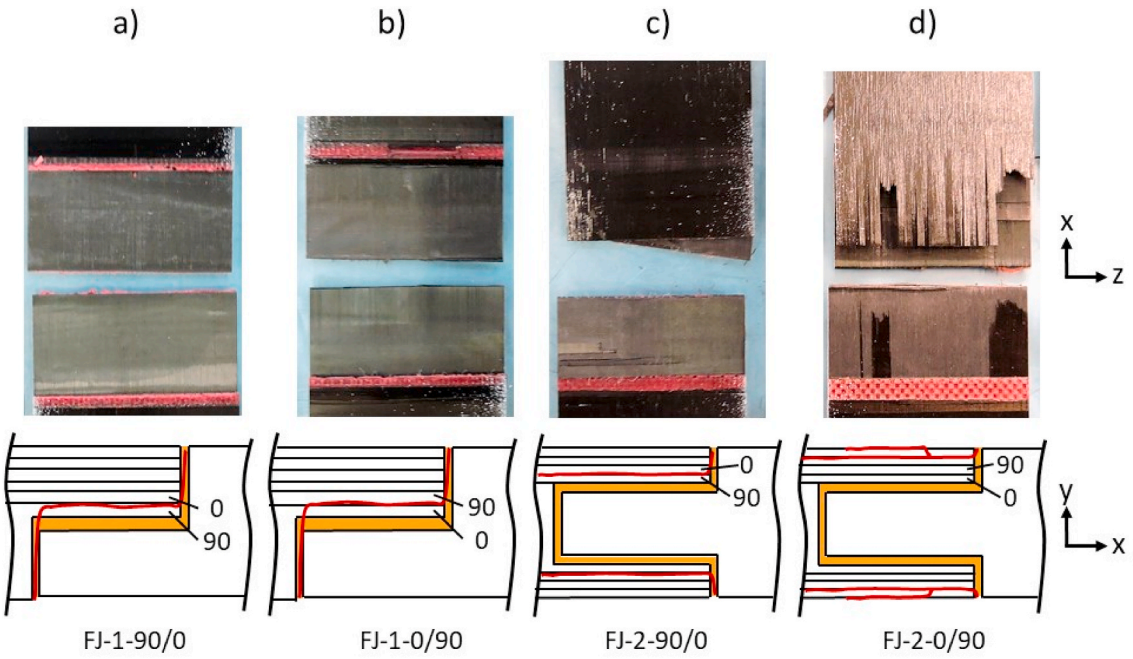

Fig. 18. Final fracture surfaces of FJ-topologies with layup $[90/0]_{4s}$ (a–b) and layup $[0/90]_{4s}$ (c–d).

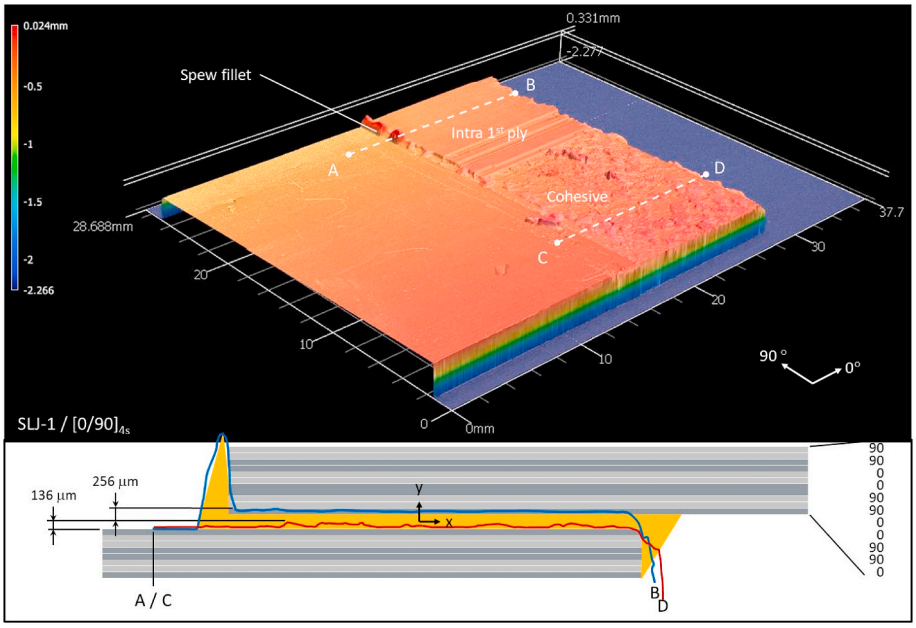

Fig. 19. Final fracture surface of a typical SLJ-1 topology in layup $[0/90]_{4s}$.

5. Discussion

5.1. Fracture surfaces: Competition between cohesive and composite failure

The topology which shows the largest cohesive fracture area is the SLJ-topology with $[0/90]_{4s}$. This result is in agreement with previous observations of the authors [13]. An interface ply of 0° in contact with the adhesive results in high shear and low peel stresses on the bond line. This stress distribution favours fracture to occur cohesively inside the adhesive, correlating well with the stress analysis in section 3.3. For the SLJ configuration with $[90/0]_{4s}$ layup, with an interface ply angle of 90°, the peel stresses are high both in the adhesive and in the composite adherend. The peel strength of the adhesive is higher than the interlaminar strength of the composite [2,22]. This favours fracture to occur inside the composite, as observed in the final fracture surfaces of SLJ-configurations with $[90/0]_{4s}$.

The failure pattern of the FJ-topologies does not follow the same trend as the SLJ-topologies. Independently from adherend stacking sequence, all final fracture surfaces reveal failure inside the composite, eventually in form of inter- and intraply matrix failure, meaning that a different failure mechanism has taken place. This different trend may be caused by the integrated topology: The FJ-topologies do not have a distinct overlap edge. It is believed, that the crack starts from the surface, at the resin pocket where the plies terminate, and then travels inside until it reaches the weakest 0/90 interface to propagate as

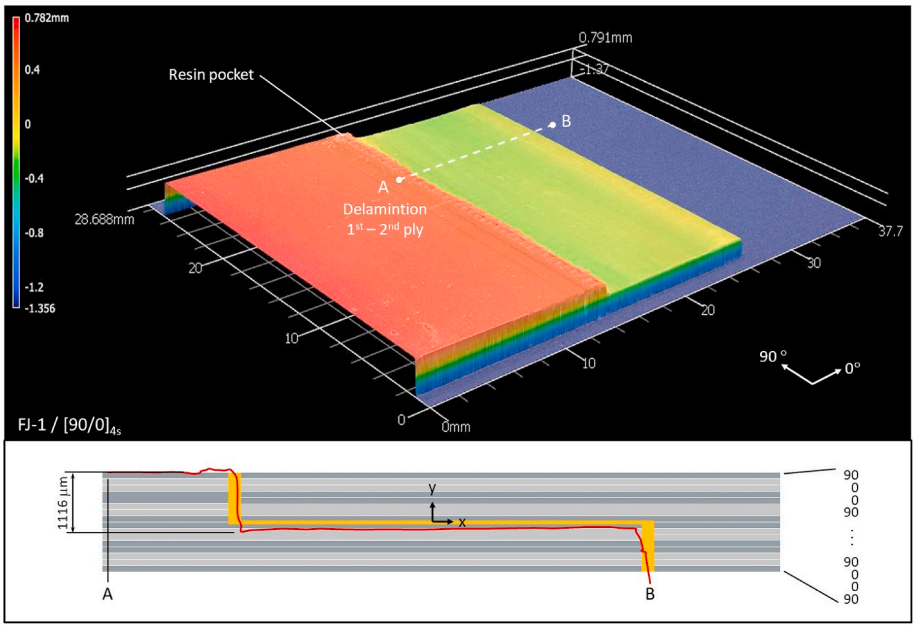

Fig. 20. Final fracture surface of a typical FJ-1 topology in layup $[90/0]_{4s}$.

delamination.

On the experimental side, it is difficult to identify only from the final fracture surfaces to which level adhesive is plastically deformed. On the numerical side, the load that has been chosen for the stress analysis is within 21% of average maximum load, for the weakest specimens in the study.

5.2. Damage initiation versus final failure

Fig. 21 shows the maximum load and work, determined from the L-d curves. The values of work per configuration correlate well to the maximum load. The highest value for maximum load is achieved with configuration SLJ-2 of layup $[0/90]_{4s}$ with average 20.03 ± 0.84 kN. It is followed by the 2-finger topologies, with FJ-2-90/0 (15.88 ± 1.29 kN) and FJ-2-0/90 (15.24 ± 2.28 kN). The lowest value is achieved by the SLJ-1 configuration with $[90/0]_{4s}$ layup (7.10 ± 0.73 kN), which is in the same range as the FJ-1 topologies, with FJ-1-90/0 (7.99 ± 0.35 kN) and FJ-1-0/90 (8.45 ± 0.75 kN).

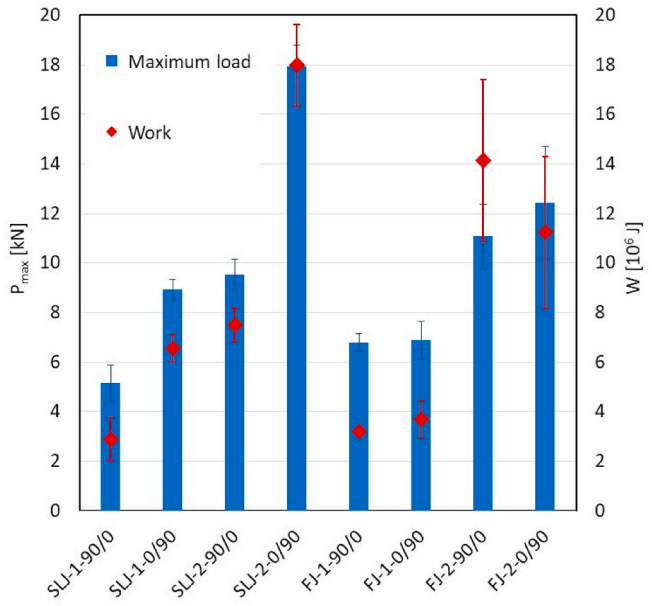

Fig. 21. a) Maximum load [kN] versus work [10^6 J] (±standard deviation).

Comparing SLJ-configurations, this result is expected, since a larger overlap length, in combination with a 0° outside layer, adjacent to the bond line lead to higher bending stiffness and thus a reduction in peel stress at the bond line - see subsection 3.3. In case of the FJ-configurations, the values for maximum load at final failure are in accordance with the numerical stress analysis in subsection 3.3: The FJ-1-configurations provide a very low maximum load, while in the FJ-2-configurations the maximum load increases significantly.

In Fig. 22, the load at damage initiation is compared to the maximum Mises stress inside the adhesive, for each configuration. Fig. 22 a) shows the load at damage initiation, which is experimentally derived via AE-monitoring - see subsection 4.3.

Comparing the plots in Figs. 21 and 22 a), the trend for load at damage initiation does not correlate to the trend for maximum load: While FJ-2-90/0 shows the lowest peel and shear stress as well as highest load at damage initiation, it is outperformed by SLJ-2-0/90 in maximum load. It is believed that a cohesive failure inside the bond line of the SLJ-2-0/90 configuration would provide higher maximum load than a delamination failure inside the adherend of the FJ-2-90/0 configuration, where the crack could propagate more suddenly. Another explanation could be, that those manufacturing flaws, resin flow-out, layer undulation and ply drops, that are mainly observed inside the FJ-topologies, shown in section 4.1.2, could possibly influence the damage evolution inside the joint. However, these defects might as well have an influence on the damage initiation rather than on the damage propagation, or at least in the same extend.

Fig. 22 b) shows the maximum Mises stress inside the adhesive, taken at a load of 1.5 kN, below damage initiation. It is shown in subsection 3.3, that the peel stresses are not the most critical for finger joints. Therefore Mises stresses give a better comparison between different topologies. Comparing Fig. 22a) and b), the two FJ-configurations, FJ-1-90/0 and FJ-1-0/90, with the lowest damage initiation load are the ones with the highest maximum Mises stress. On the other side, the FJ-2-90/0 with the highest damage initiation load corresponds to the lowest maximum Mises stress. The SLJ-configuration load at damage onset and Mises stresses are in between the FJ-1 and FJ-2. Among the SLJ-configurations, SLJ-2-90/0 has the highest damage initiation load, corresponding to the lowest maximum Mises stress. However, as the values

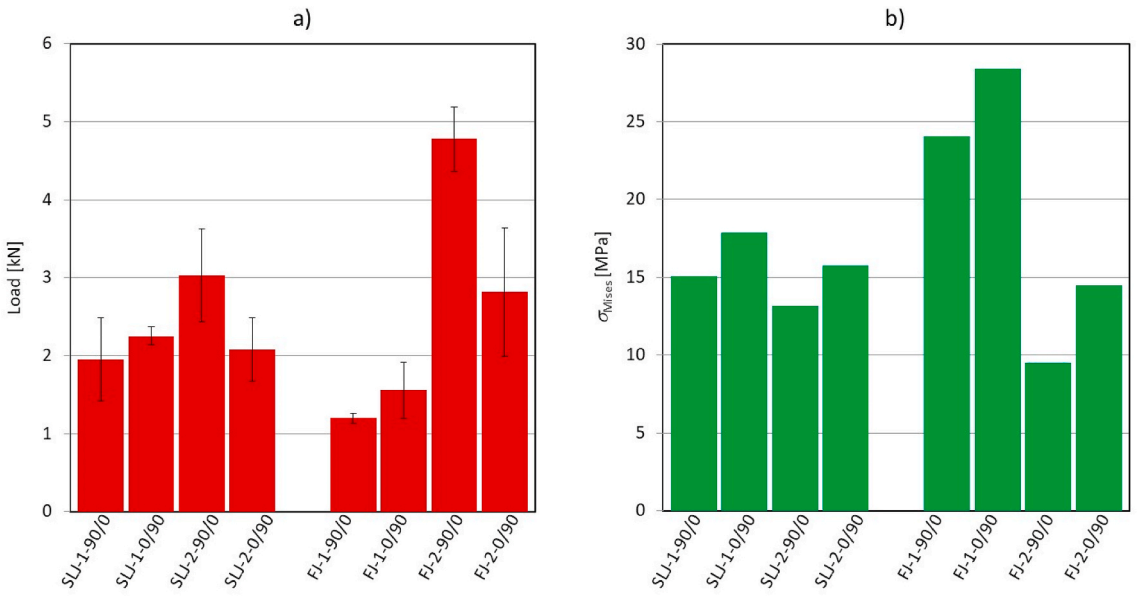

Fig. 22. a) Load at damage initiation [kN] (±standard deviation) b) maximum Mises stress inside the adhesive [MPa].

for different SLJ-configurations are in close range, the differences are less pronounced than in the FJs. Nevertheless, it can be concluded that the Mises stresses inside the adhesive is a good parameter to predict the damage onset on the joint, which indicates that the damage onset occurs inside the adhesive and not inside the composite.

It is important to note that, the adhesive thickness of the FE-model, presented in chapter 3, is based on a 50 µm bond line thickness, whereas the experimentally measured bond line thickness was confirmed with 150 µm for all specimens. This discrepancy may have an impact on the measured stress distribution in the FE-model. It is therefore expected that stresses in Fig. 23 b) would be lower with increased bond line thickness.

To further assess the location of damage initiation in the FJ- and SLJ-configurations, the Mises stress distribution is shown in Figs. 23 and 24, respectively. Both Figures show a 2D cross-section of the side of the overlap region, zoomed into the butt joint resin pocket of the FJs in Fig. 23 and into the triangular spew fillet of the SLJs in Fig. 24, where the Mises stresses are found to be the highest. The stresses are taken at a load of 1.5 kN, below damage initiation and do not change significantly along the specimen's width.

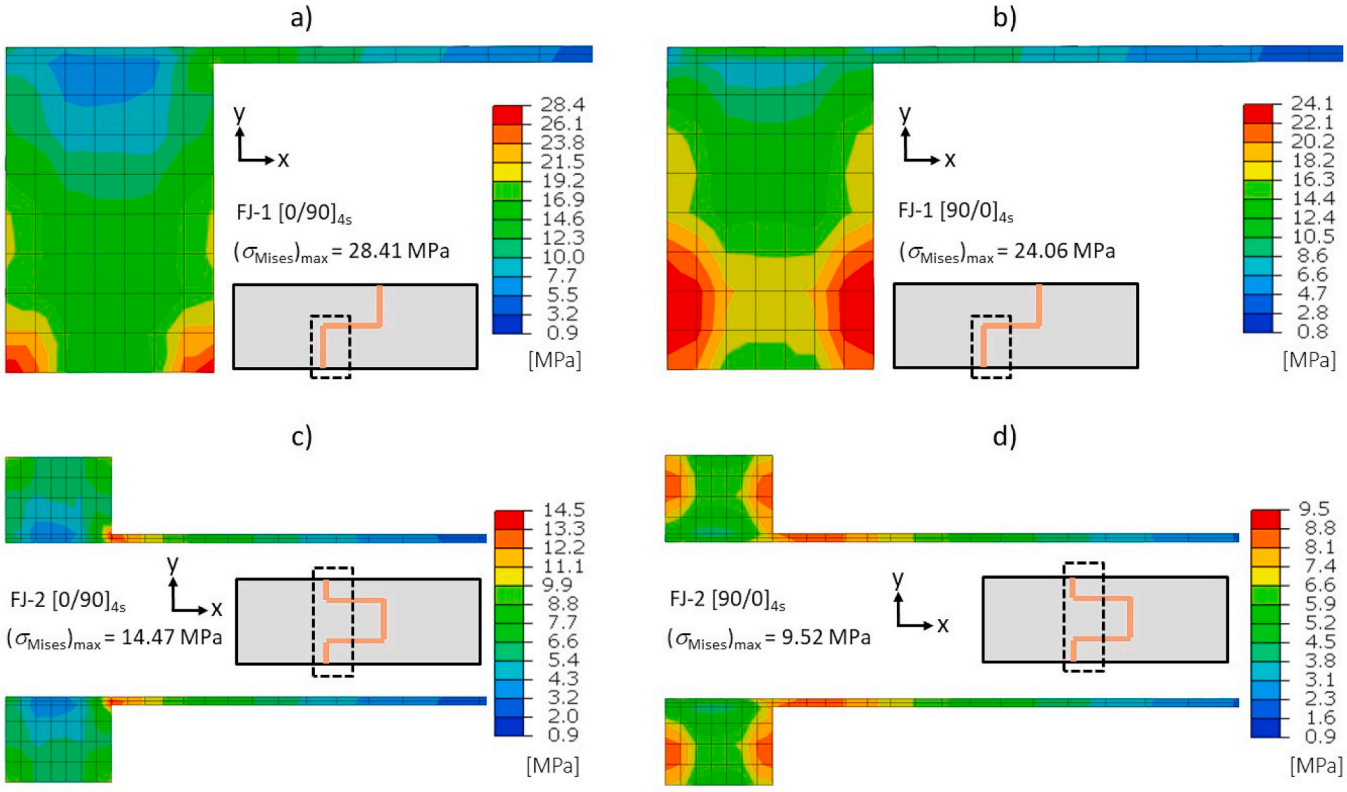

Fig. 23. Mises stress distribution in all FJ-configurations at left tip of overlap area for 1.5 kN load.

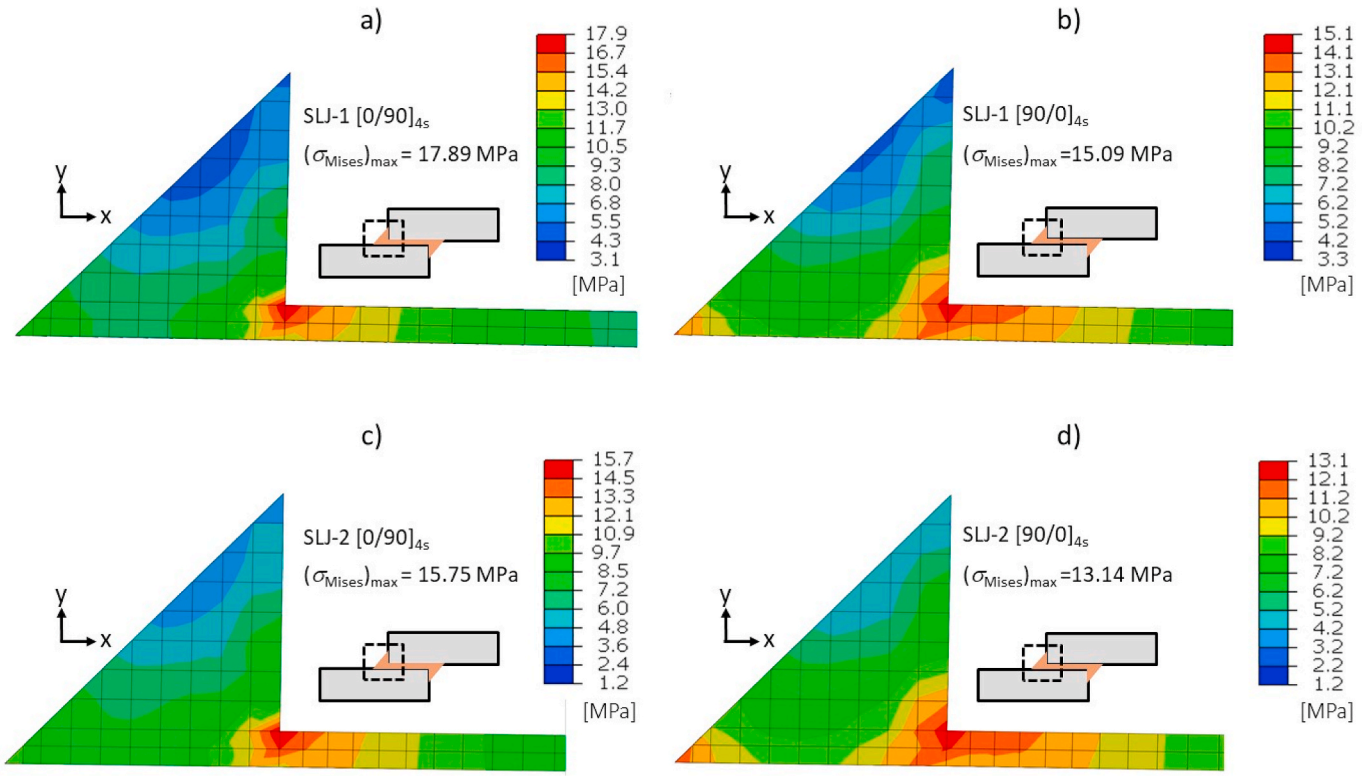

Fig. 24. Mises stress distribution in all FJ-configurations at left tip of overlap area for 1.5 kN load.

The location of maximum Mises stress in all SLJ-configurations of Fig. 24 is always observed at the corner of the fillet in contact with the upper adherend corner. This suggests that a tapering of the adherend could also decrease the peak stresses [23]. For the FJ-configurations shown in Fig. 23, the maximum Mises stresses occur inside the butt joined region. This maximum occurs in the alignement of the outer 0 °-layer of the adherend and shows that, the Mises stresses in a butt joint configuration are higher in the alignement of a 0° layer than for a 90° layer. In fact, it is not the peel or shear, but the in-plane tensile stress component, which is, for the butt region in the FJ-configurations of Fig. 24, the dominant stress component, relating to those observations on Fig. 9 in subsection 3.3. This is an interesting and complementary finding to previous conclusions from the authors, stating that 0° as an interface ply in a SLJ-configuration results in the highest shear stresses in SLJ-configuration [13]. Based on the maximum Mises stress distribution, it is therefore possible, that in the experiments, the FJs fail first in the butt joint area. However, this assumption could not be confirmed by the location of damage initiation by AE-signals or from final fracture surfaces. It can be concluded that:

1) FJ-1-topologies exhibit the lowest damage onset, corresponding with highest peel stress in the overlap region, together with highest in-plane tensile stress in the butt region. The location of maximum Mises stress in Fig. 23 confirms this.
2) FJ-2-topologies, on the other hand, have the highest damage onset, corresponding with the lowest peel stresses in the overlap region and low tensile stresses in the butt region.
3) The SLJ-topologies are between FJ-1 and FJ-2 both in experimentally derived load for damage onset and in terms of peak peel stress in the numerical analysis of section 3.3. Unlike the FJ-configurations, for the SLJ-configurations, the highest Mises stresses are dominated by peel and shear stress components. The location of maximum Mises stress in Fig. 24 does again confirm this.

5.3. Damage resistance and weight efficiency

Another comparison of the different configurations can be made, by correlating the load at damage initiation (F_{init}) and the maximum load (F_{max}). The term “damage resistance” can be proposed as

$$D = 1 - \frac{F_{init}}{F_{max}} \tag{3}$$

Yet another comparison of the different configurations can be made, by correlating the maximum load with the volume of the joint. Given weight equals volume times density, and given that the density of the CFRP-epoxy adhesive bonding area is approximately constant for all configurations, the volume of the joint overlap area V_{OL} can be described as the product of overlap length (OL) times overlap thickness (OT) times specimen width (W), and a “joint weight efficiency” can be proposed as:

$$\Theta = \frac{F_{max}}{V_{OL}} \tag{4}$$

Due to the integrated geometry, the FJ-topology configurations consequently reach higher joint weight efficiencies than the SLJ-topologies. For applications, where the structural weight is a critical parameter, such as an aircraft fuselage, a weight efficient FJ-topology may be an alternative to the conventional SLJ-topology. In fact, the weight efficiency of the FJ-topology could be further optimized, for example with a longer overlap length, than the 12.7 mm of this study, as long as manufacturability is still feasible. Table 6 describes the damage resistence and the joint weight efficiency for all configurations. The values of Table 6 result in a similar damage resistance amongst all joint configurations, ranging from 0.70 (±0.04) for the FJ-2-90/0 up to 0.90 (±0.02) for the SLJ-1-0/90 type.

A final comparison can be given as guideline for designers: With both SLJ and FJ design expected to withstand the same design load, the FJ can effectively replace the SLJ, if weight efficiency is the main requirement: If a weight efficiency Θ, as ratio of maximum load F_{max} over joint overlap volume V_{OL}, see Eq. (4), is required above a value of 7.5, the FJ-

Table 6
Damage resistance [−] and joint weight efficiency [kN/mm^3] for all configurations.

	Damage resistance	Joint weight efficiency
	$1\text{-}F_{init}/F_{max}$ [−]	$F_{max}/(OL^*OT^*W)$ [kN/mm^3]
SLJ-1-90/0	0.72 (±0.11)	5.57 (±0.69)
SLJ-1-0/90	0.80 (±0.01)	7.48 (±0.22)
SLJ-2-90/0	0.76 (±0.04)	4.39 (±0.28)
SLJ-2-0/90	0.90 (±0.02)	7.05 (±0.35)
FJ-1-90/0	0.85 (±0.00)	14.59 (±0.88)
FJ-1-0/90	0.81 (±0.04)	15.16 (±1.44)
FJ-2-90/0	0.70 (±0.04)	32.00 (±2.58)
FJ-2-0/90	0.81 (±0.06)	27.90 (±4.21)

design would be a better candidate than a SLJ-design. If the designer instead aims for a topology of absolute maximum joint strength, a FJ-design would not be the first choice.

6. Conclusion

This study aims to explore the effect of a multi-stacked finger joint topology in comparison with a conventional single overlap joint topology on the tensile strength of composite bonded joints. In total, 8 different topology configurations are studied under quasi-static tensile loading. A non-linear FE-analysis is performed to analyse the shear and peel stresses along the adhesive bond line. Experimental lapshear tests are performed and monitored using AE-technique to follow the damage events. The following conclusions can be drawn:

- A certain layup of the CFRP-adherend can steer the crack path. For a layup of $[0/90]_{4s}$, the crack propagates cohesively along the bond line for SLJ- but inside the composite for FJ-topologies.With a stacking sequence of $[90/0]_{4s}$, a crack can be triggered inside the composite for both SLJ- and FJ-topologies.
- For the FJ-1-topology the beneficial effect of avoiding eccentricity is outperformed by the detrimental effect of stiffness reduction at the overlap, such that the peak peel stresses are higher than in the SLJ-configurations. For the FJ-2-topology, the stress field changes significantly and in this case the FJ-2-topology outreaches the SLJ-topologies.
- In accordance with previous work, it was found that topologies with layup $[0/90]_{4s}$ result in higher peak shear stress but lower peak peel stress inside the adhesive bond line when compared to layup $[90/0]_{4s}$.
- The FJ-2-topology in layup $[90/0]_{4s}$, which fractures inside the adherend, provides the lowest peak shear and peel stress and the highest load at damage initiation. It is however outperformed in maximum load by the SLJ-topology with layup $[0/90]_{4s}$, which fractures cohesively inside the adhesive.
- Unlike in single overlap topologies, the most dominant stress component for damage initiation inside the FJ-design is the in-plane tensile stress, at the butt joint resin pockets, rather than peel stresses at the overlap region.
- Within this study, it was found that the von Mises stress inside the adhesive is a suitable parameter to correlate with the damage onset in bonded joints of different design configurations.
- Despite the common believe that finger joint topologies are not feasibly in terms of manufacturability, for CFRP-joints with adherend thickness below 5 mm, this study proposes a simple laminating strategy for joint topologies without eccentricity but with one or two overlaps stacked through the thickness of the joint. However, manufacturing imperfection due to resin flow-out, layup undulations and ply drops inside the adherend laminates are identified in the FJ-topologies, when compared to the SLJ topologies. Based on the descripancy between the trends at damage initation and at maximum load, it is believed that damage evolution may be affected by those manufacturing imperfections, particularly in the case of the FJ-2-topologies.
- As design guideline, FJs can effectively replace SLJs, if weight efficiency is the main requirement. However the SLJ design results in higher absolute maximum joint strength than the FJ-design.

Data availability

The data required to reproduce these findings are available to download from https://doi.org/10.4121/uuid:e250f8a1-d609-4b11-b1a7-709aa24bb2ab.

Acknowledgement

This work has been funded by the Netherlands Organisation for Scientific Research (NWO), project number 14366.

References

[1] Adams RD. Strength predictions for lap joints, especially with composite adherends. *A review*. J Adhes 1989;30:219–42.
[2] Teixeira de Freitas S, Sinke J. *Failure analysis of adhesively-bonded skin-to-stiffener joints*: metal–metal vs. composite–metal. Eng Fail Anal 2015;56:2–13.
[3] Crocombe AD, Ashcroft IA. Modelling of adhesively bonded joints. Springer; 2008, ISBN 978-3-540-79055-6 [Chapter 1]: Simple Lap Joint Geometry.
[4] SPS 1: special products standard for fingerjoined structural lumber. Vancouver: National Lumber Grades Authority; 2017.
[5] Sayer F, Antoniou A, van Wingerde A. Investigation of structural bond lines in wind turbine blades by sub-component tests. Int J Adhesion Adhes 2012;37:129–35.
[6] Ahamed J, Joosten M, Callus P, John S, Wang CH. Ply-interleaving technique for joining hybrid carbon/glass fibre composite materials. Comp.: Part A 2016;84:134–46.
[7] Dvorak GJ, Zhang J, Canyurt O. Adhesive tongue-and-groove joints for thick composite laminates. Compos Sci Technol 2001;61:1123–42.
[8] Matous K, Dvorak GJ. Analysis of tongue and groove joints for thick laminates. Composites Part B 2004;35:609–17.
[9] Canyurt OE, Meran C, Uslu M. Strength estimation of adhesively bonded tongue and groove joint of thick composite sandwich structures using genetic algorithm approach. Journal of Adhesion and Adhesives 2010;30:281–7.
[10] Sen I. Design of A350 XWB Aircraft fuselage design study: parametric modelling, structural analysis, material evaluation and optimization for aircraft fuselage. Master thesis at Delft University of Technology, Faculty of Aerospace Engineering; 2010.
[11] Uhlmann E, Sammler F, Richarz S, Heitmueller F, Bilz M. Machining of carbon fibre reinforced plastics. Procedia CIRP 2014;24:19–24.
[12] ASTM D5868 01. Standard test method for lap shear adhesion for fiber reinforced plastic (FRP) bonding. 2014.
[13] Kupski J, Teixeira de Freitas S, Zarouchas D, Camanho P, Benedictus R. Layup variation Composite layup effect on the failure mechanism of single lap bonded joints. Compos Struct 2019;217:14–26.
[14] Kaw K. Mechanics of composite materials. Boca Raton: Taylor & Francis; 2006.
[15] Material datasheet: *a75-T-2-0123-1-1*. Airbus Material-Handbook Structure; 2014.
[16] Camanho PP, Arteiro A, Melro AR, Catalanotti G, Vogler M. Three-dimensional invariant-based failure criteria for fibre-reinforced composites. Int J Solid Struct 2015;55:92–107.
[17] Teixeira de Freitas S, Zarouchas D, Poulis JA. The use of acoustic emission and composite peel tests to detect weak adhesion in composite structures. J Adhes 2018;94:743–66.
[18] datasheet Material. *Scotch-Weld™ structural adhesive film AF 163-2AF163-2k*. 3M, Multimedia database; 2009.
[19] J. Kupski, D. Zarouchas, S. Teixeira de Freitas: Thin-plies in adhesively bonded carbon fiber reinforced polymers. Composites Part B, vol. 184, 2020.
[20] Ultraviolet-ozone surface treatment. Three Bond Technical News; 1987.
[21] Poulis JA. *Small cylindrical adhesive bonds*. PhD thesis. The Netherlands: Technical University Delft; 1993, ISBN -90370-0082-7. p. 39–62.
[22] Teixeira de Freitas S, Sinke J. Adhesion properties of bonded composite-to-aluminium joints using peel tests. J Adhes 2014;90:511–25.
[23] Shang X, Marques E, Machado J, Carbas R, Jiang D, da Silva L. Review on techniques to improve the strength of adhesive joints with composite adherends. Composites Part B 2019;177.